A RESONANT CAVITY METHOD OF MEASURING THE VELOCITY OF LIGHT

Thesis by

Harry Gruenberg

In Partial Fulfillment of the Requirements
For the Degree of
Doctor of Philosophy

California Institute of Technology
Pasadena, California

1949

Acknowledgments

The work described herein was carried out under the helpful supervision of Professor W.H. Pickering. Acknowledgments are also due to Professor W.R. Smythe for his many suggestions.

Abstract

A method is proposed to determine the velocity of propagation of electromagnetic waves by means of a resonant cavity. A circular cylindrical cavity is used operating in the TE_{011} mode. It is shown that for a particular length-to-diameter ratio, the resonance frequency is only a function of the cavity volume and the velocity of electromagnetic waves. The latter can be calculated, when resonance frequency and cavity volume are determined experimentally. The main advantage of this method is, that the volume has to be measured only to one-third the accuracy which is desired for the propagation velocity. Linear dimensions, on the other hand, have to be determined to the same accuracy. Furthermore, the volume method requires only reasonable tolerances in the construction of the cavity.

The effects of various cavity imperfections on the resonance frequency were analysed. The frequency shifts due to the finite conductivity of the walls, the deformations in the boundary surface, grooves, and coupling irises, were calculated. The problem of a thick iris was treated numerically.

Preliminary experiments on a silver-plated brass cavity led to a result of

$$299{,}764 \pm 15 \text{ km/sec.}$$

This is somewhat lower than the presently accepted value of the velocity of light, but is in substantial agreement with that value within the limits of experimental error.

A discussion of the various sources of error indicates that an ultimate accuracy of 1 part in 150,000 is quite possible.

Table of Contents

List of Illustrations

I. Historical Survey

The velocity of light is probably the most fundamental physical constant. A knowledge of its exact value is of great importance because many other physical constants are derivable from or related to it.

Successful attempts to estimate the velocity of light date back to the seventeenth century (1,2). The first crude determinations were based on astronomical observations. Olaf Römer in 1675 correctly attributed the slight variations in the periods of revolution of Jupiter's satellites to the finite velocity of propagation of the sunlight reflected from these satellites. Römer's work was discredited for many years until finally James Bradley's discovery of the aberration of stars in 1727 led to a new and independent method of estimating the velocity of light. All astronomical methods require a knowledge of the distance between the Sun and the Earth which is not known with sufficient accuracy even today to rival terrestrial determinations.

Two terrestrial methods were introduced by Fizeau (1849) and Foucault (1850). All direct terrestrial methods used to date are improvements and modifications of Fizeau's cogwheel method or Foucault's rotating mirror experiment. A great many determinations were made during the latter half of the nineteenth century by Cornu, Young, Newcomb, Michelson, and others. None of these approached the precision obtained during the last few decades (1,2,3, and 4).

A.A. Michelson (5) conducted a new series of investigations from 1921 to 1926. He used rotating mirrors of 8,12, and 16 sides and a path length of about 45 miles between Mount Wilson and Mount San Antonio. His final result is quoted as 299,796 ± 4 km/sec. The high precision attributed to the result is not quite justified because of the uncertainty in atmospheric conditions and possibly in the path length which had to be obtained by triangulation over mountainous terrain. Because of these uncertainties, Michelson, Pease, and Pearson (6) repeated the experiments (1929 to 1933) in an evacuated, mile-long steel pipe. The effective path length was increased to 10 miles by multiple reflections from two plane mirrors. A number of rotating mirrors of 32 sides were used. The mean of 2885 determinations was 299,774 km/sec. Although individual results show a considerable spread (about ±29km), the mean values obtained by different mirrors and at different times are in remarkable good agreement. The probable error of a single observation is given as ±9 km/sec, with the probable error of the mean considerably less than ±1 km/sec.

A modified form of the cogwheel experiment was used by Karolus and Mittelstaedt (7) about 1925. In their experiment the "shutter effect" of the teeth of the wheel was reproduced by Kerr cells placed between crossed Nicol prisms. In this manner they were able to use shutter frequencies as high as 7 megacycles per second, compared to 50,000 cycles per second as used by Fizeau. This permits a considerable reduction in path length. The final result for a path length of approximately 300 meters was 299,778 ± 10 km/sec.

Anderson (8,9) used the rotating mirror method in two series of determinations (1937 and 1941) in which additional refinements were introduced. His 1941 result is given as 299,776 ± 14 km/sec. This includes a correction due to the difference in group and phase velocity which had been overlooked by earlier investigators. The necessity of this correction was pointed out by Birge (9).

Various indirect determinations of the velocity of light have been made since 1900. In some of these determinations, a degree of precision has been achieved which is almost comparable to that obtained by direct methods.

From electromagnetic theory, the ratio of the charge on a condenser measured in ~~the~~ electrostatic units to that measured in electromagnetic units, should be numerically equal to the velocity of light. The best value for this ratio was obtained by Rosa and Dorsey (10) in 1907. Their result was given in terms of the international ohm. Taking account of the discrepancy between international and absolute ohm, Birge (11,12) quotes their corrected result as 299,784 ± 10 km/sec.

A number of experimenters have deduced the value of the velocity of light from an investigation of the standing electric waves along parallel wires. Mercier (13) obtained a value of 299,782 ± 30 km/sec in 1923. This is in excellent agreement with Rosa and Dorsey's result, although the large corrections required make Mercier's result comparatively uncertain.

Essen and Gordon-Smith (14) have applied resonant cavity techniques for the first time to a precision measurement of the velocity of propagation of electromagnetic waves. They use a circular cylindrical cavity excited by a probe from a coaxial line. The resonance frequency is determined by adjusting the frequency for maximum cavity transmission. Dimensions are measured by interferometer comparison with wrung Johnson guage blocks. These measurements are made at a number of points on the cavity circumference and averages are used. Their results (1948) are not too consistent and differ somewhat, depending on the mode of oscillation used. Best results are claimed for the TM_{010} and TM_{011} modes and the value finally adopted is 299,792 ± 9 km/sec which exceeds Michelson's most recent result by 18 km/sec. Averages for the TE_{011} and TE_{111} modes are given as 299,799 and 299,777 km/sec, respectively. Hence, further investigation in this direction seems indicated.

The presently accepted value for the velocity of light is that adopted by Birge (12) in 1941, namely

299,776 ± 4 km/sec.

It is a weighted average of the results obtained by Michelson, Pease, and Pearson; Anderson, and Rosa and Dorsey.

II. Survey of Cavity Methods

The resonance frequency of a cavity resonator depends on the internal dimensions of the cavity, the propagation velocity of electromagnetic waves in the dielectric filling the cavity, and the type of mode excited in it. Hence, if the dimensions of the cavity and its resonance frequency for a particular mode are measured, the propagation velocity can be determined. In principle, it is not difficult to measure the resonance frequency of an actual cavity to within one part in a million, but corrections have to be applied for the finite conductivity of the walls, the effect of the coupling mechanism, and possibly for deviations from the ideal cavity shape. The measurement of the internal dimensions of the cavity to the same degree of accuracy appears more difficult, although it is conceivable that interferometer methods could be applied. The construction of a cavity to that precision certainly poses a problem.

For practical reasons and ease of construction a circular cylindrical cavity was chosen. Such a cavity can be very accurately machined by making it out of three parts: a cylindrical main body and two flat end plates. If a circular transverse-electric mode (TE_{onp}) is excited in it, there will be no wall currents crossing the joints between the three parts and hence no good electrical contact will be necessary. Such a mode will have a very high Q and hence only a small correction to the measured resonance frequency will be required.

For a circular cylindrical cavity excited in a TE_{onp} mode the ideal resonance frequency is given by (15,16)

$$f = c\sqrt{\left(\frac{r_{on}}{\pi D}\right)^2 + \left(\frac{p}{2L}\right)^2} \tag{2.1}$$

where

c = propagation velocity of electromagnetic waves

D = diameter of the cavity

L = length of the cavity

r_{on} = nth root of $J_o'(x) = 0$.

This assumes, of course, that the inside walls of the cavity form a mathematically accurate right circular cylinder and that the wall material has infinite conductivity. Also any effects of coupling holes or loops are neglected.

It is apparent that the precision with which the internal cavity diameter can be determined will be lower than that achievable for the length. For high accuracy it will therefore be of advantage to eliminate D from equation (2.1). This can be done in at least three ways:

(a) The length of the cavity can be made variable by a movable piston at one end. For a fixed frequency the resonant lengths can be determined for two or more modes; for example, the TE_{o11} and TE_{o21} modes. From two equations of the form (2.1) the diameter can be expressed in terms of two resonant length.

(b) For a cavity of fixed dimensions the resonance frequency for two modes can be measured. This makes it possible to determine the ratio D/L very accurately.

(c) If the volume of the cavity is measured instead of its linear dimensions, it can be shown that the resonance frequency is independent of the length-to-diameter ratio if this ratio is chosen to be

$$\rho_o \triangleq \frac{L}{D} = \frac{\pi}{\sqrt{2}} \frac{p}{r_{on}} \qquad (2.2)$$

This ratio is not too critical and it will be shown later that even a construction error as large as $\frac{1}{2}$ per cent will lead to a negligible error in the result if the effect of the length-to-diameter ratio is neglected.

It is doubtful whether the first method will lead to any higher accuracy than a direct measurement of D and L in a fixed cavity. Although the diameter measurement is replaced by another length measurement, the constructional difficulties and the difficulties in accurately measuring the lengths would certainly be increased. By using three resonant modes and measuring only changes in length by interferometer methods these difficulties can possibly be circumvented.

The second method seems to be intrinsically more accurate. Only one length measurement is required, the diameter measurement being replaced by another frequency determination. This method requires, however, power sources for two different frequencies and a secondary frequency standard variable over a large frequency range. Furthermore, the cavity must be machined to very close tolerances. The end plates must be optically flat and accurately parallel. An elaborate and expensive setup is necessary to determine the exact distance between end plates. The ultimate limit of this method will probably be set by the accuracy with which corrections to the resonance frequency can be determined, especially the correction due to coupling holes.

The third method certainly surpasses the other two in simplicity. No extreme accuracy in the construction of the cavity is necessary because the resonance frequency is comparatively insensitive to slight deformations or imperfections in the cavity walls provided that the cavity volume is kept constant. A frequency standard the frequency of which is variable over a small fraction of a per cent only is required. No elaborate setup for measurement of linear dimensions is necessary and the expenditure of time and money is kept within reason. The ultimate accuracy of this method is limited by the accuracy with which the internal cavity volume can be determined. With sufficient care it should be possible to measure this volume to perhaps 1 part in 50,000. The velocity of electromagnetic waves could then be determined to an accuracy of about 1 part in 150,000. This is approximately the probable error in the presently accepted value for the velocity of light and better than the probable error in any single determination made so far.

To obtain the same accuracy with the first two methods, linear dimensions have to be determined to 1 part in 150,000.

To see whether it is possible to get at least the same accuracy in the determination of the resonance frequency, it is first necessary to analyse the effect of the coupling holes, since they cause by far the largest shift in the ideal resonance frequency. If it is assumed that this shift can be calculated or measured to within a few percent only, then the coupling holes must be kept small enough so that they do not shift the frequency by more than 1 or 2 parts in 10,000. This places a serious limitation on the power transmission through the cavity. It was found experimentally, however, that with the available microwave power sources sufficient power could be transmitted through the cavity to make good detection possible.

For the above reasons, the last method was adopted.

III. Theory of Proposed Method

In terms of the cavity volume V and the length-to-diameter ratio ρ, the cavity dimensions can be written in the form

$$D = \sqrt[3]{\frac{4V}{\pi\rho}} \tag{3.1}$$

$$L = \rho D = \sqrt[3]{\frac{4V\rho^2}{\pi}} \tag{3.2}$$

Substituting these expressions into equation (2.1) and solving for c, one obtains

$$c = \frac{f}{r_{on}} \sqrt[3]{4\pi^2 V} \frac{\sqrt[3]{\rho^2}}{\sqrt{\rho^2 + \left(\frac{\pi p}{2 r_{on}}\right)^2}} \tag{3.3}$$

This result shows, as can of course be expected, that to obtain a given accuracy for the velocity c, the resonance frequency must be known to the same accuracy, but the volume need be known to only one third of this accuracy. It is of greater interest, however, to investigate the dependence on ρ. Partial differentiation with respect to ρ yields:

$$\frac{\partial c}{\partial \rho} = \frac{f}{3 r_{on}} \left(\frac{4\pi^2 V}{\rho}\right)^{1/3} \frac{2\left(\frac{\pi p}{2 r_{on}}\right)^2 - \rho^2}{\left[\left(\frac{\pi p}{2 r_{on}}\right)^2 + \rho^2\right]^{3/2}}$$

The fractional error in c due to a given fractional error in the measured value of ρ is then

$$\frac{\Delta c}{c} = \frac{\rho}{c} \frac{\partial c}{\partial \rho} \frac{\Delta \rho}{\rho} = \frac{2}{3} \frac{\rho_0^2 - \rho^2}{\rho_0^2 + 2\rho^2} \frac{\Delta \rho}{\rho} \tag{3.4}$$

where

$$\rho_0 = \frac{\pi}{\sqrt{2}} \frac{p}{r_{on}} \tag{3.5}$$

This error can be made to vanish by choosing the length-to-diameter ratio equal to ρ_0. The physical meaning of this is, of course, that for this particular cavity shape the resonance frequency is only a function of the cavity volume and not of the ratio of length to diameter. For such a cavity equation (3.3) reduces to

$$c = \frac{f}{\sqrt{3}}\left(\frac{16\pi V}{\rho\, r_{on}^2}\right)^{1/3}. \qquad (3.6)$$

The above ratio is not too critical. If an error in ρ is made when constructing the cavity such that the true value differs from the ideal value ρ_0 by an amount $\delta\rho$, then by equation (3.4) the fractional error in c will be

$$\frac{\Delta c}{c} = \frac{2}{3}\,\frac{\rho_0^2-(\rho_0+\delta\rho)^2}{2(\rho_0+\delta\rho)^2+\rho_0^2}\,\frac{\Delta\rho}{\rho_0}.$$

Neglecting $\delta\rho$ compared to ρ_0 in the denominator and dropping the term $(\delta\rho)^2$ in the numerator, one obtains

$$\frac{\Delta c}{c} = -\frac{4}{9}\left(\frac{\delta\rho}{\rho}\right)\left(\frac{\Delta\rho}{\rho}\right). \qquad (3.7)$$

The relative error in c is less than half the product of the relative errors in ρ due to construction and due to measurement. Since the cavity can certainly be built to a tolerance better than 1 part in 1,000 and its dimensions can be measured to at least that accuracy, the above error is entirely negligible. If it is found that the actual ρ differs from the ideal value by $\Delta\rho$ then, from (3.7), equation (3.6) must be multiplied by a correction factor

$$1 - \frac{4}{9}\left(\frac{\Delta\rho}{\rho}\right)^2.$$

For an accuracy of 1 part in 150,000 this correction may be neglected for values of $\frac{\Delta\rho}{\rho} < 1/250$.

By means of (3.5) and (3.6) and the relation $c = \lambda f$, equations (3.1) and (3.2) can be re-written in the form

$$L = \frac{\sqrt{3}}{2} \rho \lambda \tag{3.8}$$

$$D = \frac{\sqrt{3}}{2} \frac{r_{0n}}{\pi} \lambda \tag{3.9}$$

These expressions give the cavity dimensions in terms of the resonant wave length subject to condition (3.5).

For the TE_{011} mode, $n = p = 1$ and $r_{01} = 3.8317060$. Hence:

$$\rho_0 = \frac{\pi}{\sqrt{2}\, r_{01}} = 0.5797525 \tag{3.10}$$

$$L = \frac{\sqrt{3}}{2} \lambda = 0.8660254\, \lambda \tag{3.11}$$

$$D = \frac{L}{\rho_0} = 1.4937840\, \lambda \tag{3.12}$$

$$c = 0.8701640\, f \sqrt[3]{V} \tag{3.13}$$

From (3.8) and (3.9) it is seen that the cavity dimensions will depend on the choice of mode and the resonance wave length. The selection of the operating wave length is mainly governed by the available microwave sources, but the size of the cavity volume also plays an important role.

Since the cavity has to be copper plated or silver plated on the inside to obtain a large Q value, the only feasible method for determining the cavity volume appears to be the weighing of the amount of distilled water that can be held by the cavity. Mercury may lead to better accuracy because of its larger density but it would attack copper or silver walls. Assuming that the weight of water filling the cavity can be determined to 1 milligram, a cavity volume of at least 50 cubic centimeters must be used to obtain an accuracy of 1 part in 50,000. From (3.8) and (3.9)

$$V = \frac{\pi}{4} D^2 L = \frac{3\sqrt{3}}{16\pi} p\, r_{on}^2 \lambda^3$$

For the lowest order TE mode (TE_{011})

$$V = 1.52\, \lambda^3$$

Because of the above requirements a wave length of at least 3.2 centimeters should be used. The use of 10-centimeter waves was not feasible as this would require a minimum volume of about 1500 cubic centimeters, which could not be measured accurately on available precision balances.

IV. Apparatus and Measuring Technique

1. Frequency Measuring Apparatus

The method of measuring the resonance frequency was similar to that described by Gaffney (17). A frequency-modulated microwave generator supplies power to the cavity (see Fig. 1). The power transmitted through the cavity is detected by a silicon crystal, amplified, and fed to the vertical-deflection plates of a cathode-ray oscilloscope. The resonance curve of the cavity is thereby displayed on the screen of the oscilloscope. The microwave generator also serves as the local oscillator in a superheterodyne receiver. It is beaten against a harmonic of a standard quartz crystal oscillator in a microwave mixer. The mixer output is fed to an intermediate-frequency receiver which passes signals only when the local oscillator frequency differs from the standard frequency by the intermediate frequency. The two side bands produced in this manner are detected and fed to the intensifier grid of the oscilloscope where they appear as two bright (or dark) dots separated by twice the intermediate frequency. The dots are superimposed on the resonance curve of the cavity. The distance between them can be adjusted by varying the intermediate frequency. By slightly changing the crystal oscillator frequency, their position relative to the resonance peak can also be varied to some extent. The resonance frequency of the cavity is exactly equal to a multiple

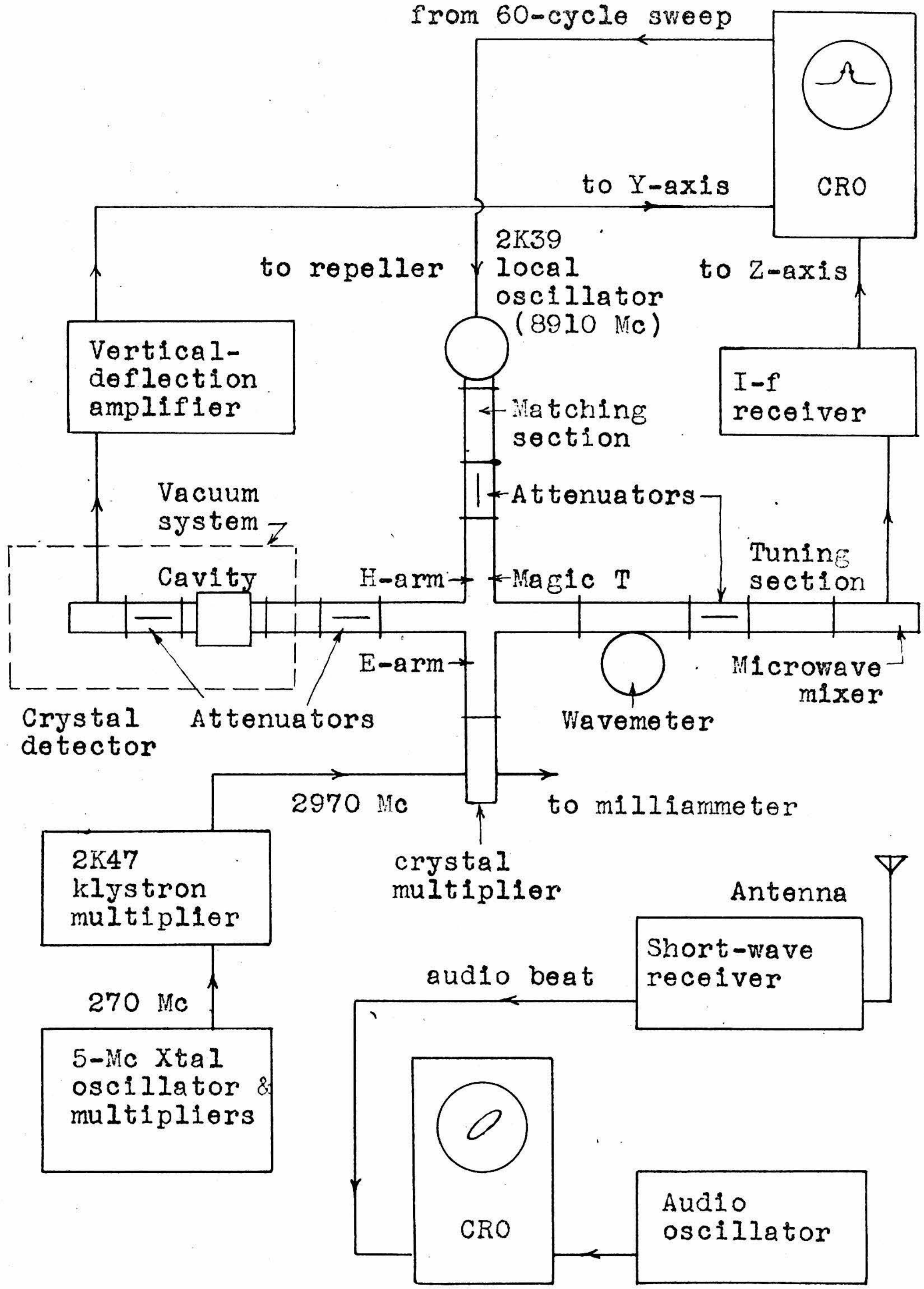

Fig. 1. Schematic diagram of frequency measuring apparatus.

of the crystal frequency when the dots are on a horizontal line on opposite sides of the peak. This frequency comparison is particularly sensitive when the dots are placed at the half-power points on the steepest portions of the resonance curve. A precision of about $\pm 1/100$ Q' is possible in this manner. In this case the loaded cavity Q can also be determined to within about 5 per cent from the bandwidth as read directly from the frequency dial of the intermediate-frequency receiver. This assumes, of course, that the detector crystal and the frequency dial on the receiver are properly calibrated.

The secondary frequency standard consisted of a 5-megacycle crystal oscillator and a chain of frequency multipliers. A nominal base frequency of 5 megacycles per second was chosen to simplify comparison with standard frequency broadcasts from radio station WWV at Beltsville, Md., near Washington, D.C. (18). The quartz crystal was enclosed in a heat-insulated box and its temperature could be thermostatically controlled. A condenser in parallel with the crystal made slight adjustments in the crystal frequency possible. Conventional class-C triplers and one doubler were used to bring the frequency up to 270 megacycles. The final stage consisted of a type 832A beam power amplifier operating in push-pull. It was driven at 90 megacycles from two 6C4 miniature triodes. The output tank circuit was constructed of $\frac{1}{4}$-inch copper tubing and tuned to 270 megacycles by means of a shorting bar. A power output of approximately 2 watts was available.

This power was used to drive a type 2K47 Sperry klystron with the aid of a small pick-up loop and a 50-ohm coaxial cable. The 2K47 klystron is a velocity modulation frequency multiplier (19). It requires an input power of from 1 to 4 watts at frequencies between 250 to 280 megacycles. The output cavity can be tuned to the ninth, tenth, eleventh, or twelfth harmonic of the input frequency. The 270-megacycle input frequency was selected to obtain optimum power output. For the same reason the output cavity was tuned to the eleventh harmonic of the input frequency. This gave about 100 milliwatts output power at a nominal frequency of 2970 megacycles. The tuning was checked by a 10-centimeter coaxial wavemeter.

To reach the 3-centimeter region, a further tripling of the frequency was required. This was achieved by a 1N21 silicon crystal mounted across a standard 3-centimeter wave guide. Because of its non-linear characteristics, the crystal will pass a current rich in harmonics. The cut-off property of the guide does not permit propagation of the fundamental and second-harmonic frequencies so that mainly third-harmonic (8910-megacycle) power is transmitted. Provisions were made to measure the d-c crystal current. Currents of 1 to 2 milliamperes were found to be satisfactory even though the conversion loss from fundamental to third-harmonic power is quite large.

A type 2K39 reflex klystron was used for the local oscillator. It was tuned to about 8910 megacycles and frequency modulated by modulating the repeller voltage with the 60-cycle saw-tooth sweep from the oscilloscope. The use of the 60-cycle sweep has the advantage that small stray pick-up voltages from the vertical-deflection amplifier are not too objectionable. Furthermore, the band width requirements for the intermediate-frequency receiver necessitate a low sweep frequency as will be shown later. The output from the local oscillator was about 200 milliwatts. The frequency deviation could be varied from zero to several megacycles.

The local oscillator signal and the standard frequency signal were combined in a magic T. The two signals were fed into the H-arm and E-arm, respectively, to avoid coupling between the two oscillators and frequency pulling of the standard. Conversion to intermediate frequency took place in a 1N23 crystal mixer. The crystal was matched to the guide by a shorting plunger and two tuning screws. An attenuator was placed between the magic T. and the mixer to avoid excessive crystal currents. Arrangements were made to use the mixer crystal as a detector for preliminary adjustments of the equipment and tuning of the local oscillator. For the same purpose a 3-centimeter absorption wavemeter was attached to a section of the guide.

The test cavity was placed between two attenuators to prevent frequency pulling by external reactance. The attenuator between magic T and cavity also served to provide a matched load to the magic T. As will be shown later, almost all the power incident on the cavity from the wave guide is reflected. Without the attenuator the magic T would thereby be seriously unbalanced and its primary purpose would be defeated.

The power transmitted through the cavity was detected by a sensitive 1N23B crystal. The detected signal was fed to the vertical-deflection amplifier through a shielded cable. To minimize 60-cycle pick-up the amplifier was operated entirely on direct current from batteries and the input stages were shielded. The first tube was shock-mounted to reduce microphonics. Particular attention also had to be given to the grounding system. It was found necessary to have a common ground for all equipment at the vertical-deflection amplifier and to move all power supplies as far as possible.

To get a faithful reproduction of the resonance curve of the cavity, sufficient band width must be allowed for in the amplifier design. For a 60-cycle sweep this is no problem as any good audio amplifier will do. The test cavity had a band width at resonance of about 300 kilocycles. The local oscillator frequency should sweep through a band of at least 2 or 3 megacycles to get the complete resonance curve on to the oscilloscope screen. The signal changes most rapidly near the half-power points. The amplifier should be able to follow these changes in a time interval corresponding to about 1/40 of the cavity band width if this band width is to be reproduced to within 5 per cent. For a 60-cycle sweep this time interval will be about 1/24,000 second and therefore, the amplifier should be designed to have a flat response from about 30 to 12,000 cycles.

The band width requirements on the intermediate-frequency receiver are not as easily met. The high accuracy in the frequency measurement can by achieved only if the intermediate- frequency dots are quite sharp. This requires that the width of the intensifier pips be very small compared to the cavity band width. Hence, the receiver must pass a band of 150 kilocycles or more. Since this is of the same order of magnitude as the intermediate frequency some compromise has to be made.

The intermediate-frequency receiver used was an adaptation of an ordinary communications receiver operating between 15 and 600 kilocycles. Only the first radio-frequency stage was used. This was followed by two further r-f stages, a conventional diode detector, and a wide-band audio stage. Satisfactory operation was obtained for intermediate frequencies above 200 kilocycles. Below that frequency the intensifier pips broadened and eventually overlapped.

Radio station WWV was received at 5 megacycles on a short-wave receiver. The antenna also picked up radiation from the crystal oscillator. The resulting audio beat was compared with the output of a calibrated audio oscillator on a second cathode-ray oscilloscope.

Cavity and crystal detector were placed under a bell jar so the resonance frequency could be measured in a vacuum. The input wave guide entered the bell jar through a rubber stopper sealed with a beeswax-rosin mixture. The guide itself was closed off with a thin polystyrene plate and sealed in a similar manner.

2. The Cavity

A preliminary cavity was made of brass and silver plated on the inside. Some advantages could be gained by using steel for the cavity material: the coefficient of thermal expansion is less (about 11×10^{-6} compared to 19×10^{-6} per degree centigrade), the strength and rigidity is higher, the weight is somewhat less, and it can be machined to closer tolerances by grinding. No particular advantage would arise from the use of invar steel, in spite of its low coefficient of expansion. It is difficult to machine and samples free of internal defects due to casting are not easily obtained. Furthermore, unless the experiment is carried out at or near 4 degrees centigrade, the large coefficient of expansion of water requires an exact knowledge of the temperature anyway. The correction due to thermal expansion can then be calculated with sufficient accuracy even for a brass cavity.

The internal cavity dimensions were calculated to make the actual resonance frequency in a vacuum equal to the frequency of the secondary standard. By comparison with standard signals from WWV, the 5-megacycle quartz crystal was found to be about 1400 cycles below its nominal frequency. This amounts to 2.5 megacycles at the 3-centimeter level. The cavity, therefore, had to be designed for 8907.5 megacycles. Adding 1.15 megacycles for the frequency shift due to the coupling holes and 0.15 megacycles for the effect of the finite conductivity of the walls (see parts V and VI), one obtains a required ideal resonance frequency of 8908.8 megacycles in vacuo. Using the presently accepted value of the velocity of light, the corresponding wave length is 3.3650 centimeters. Hence, from (3.11) and (3.12) the cavity dimensions should be:

$$D = 5.0266 \text{ cm} = 1.9790 \text{ inches}$$

$$L = 2.9142 \text{ cm} = 1.1473 \text{ inches}$$

The actual mean cavity dimensions, as measured after the plating, were

$$D = 1.9793 \text{ inches}$$

$$L = 1.1464 \text{ inches}$$

with maximum variations of 0.0005 inches.

The main cavity body was constructed with comparatively heavy flanges to make it as strong as possible (see Fig. 2 to 4). Short wave guide sections were soldered on in such a manner as to further increase the rigidity. This was necessary because the wall thickness was only 1 millimeter thick at the coupling holes. The hole diameters were 0.140 inches. The holes were tapered with a half-angle of 41 degrees to approach the "infinitely thin sheet case"

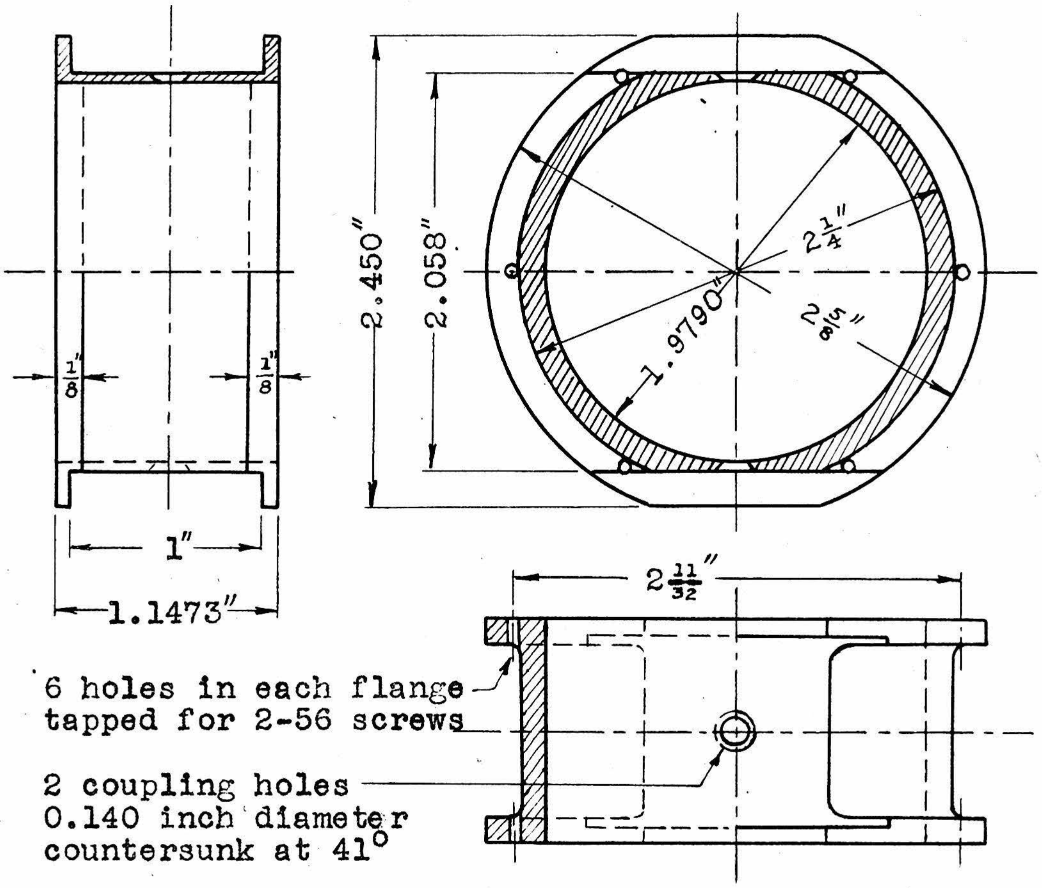

Fig. 2. Cavity main body.

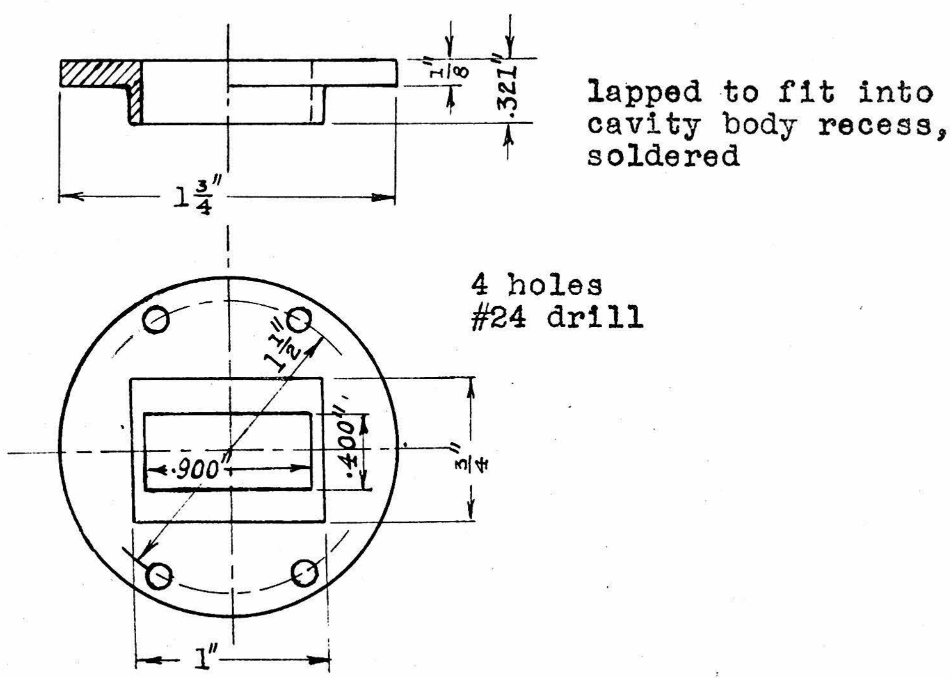

Fig. 3. Wave guide flanges.

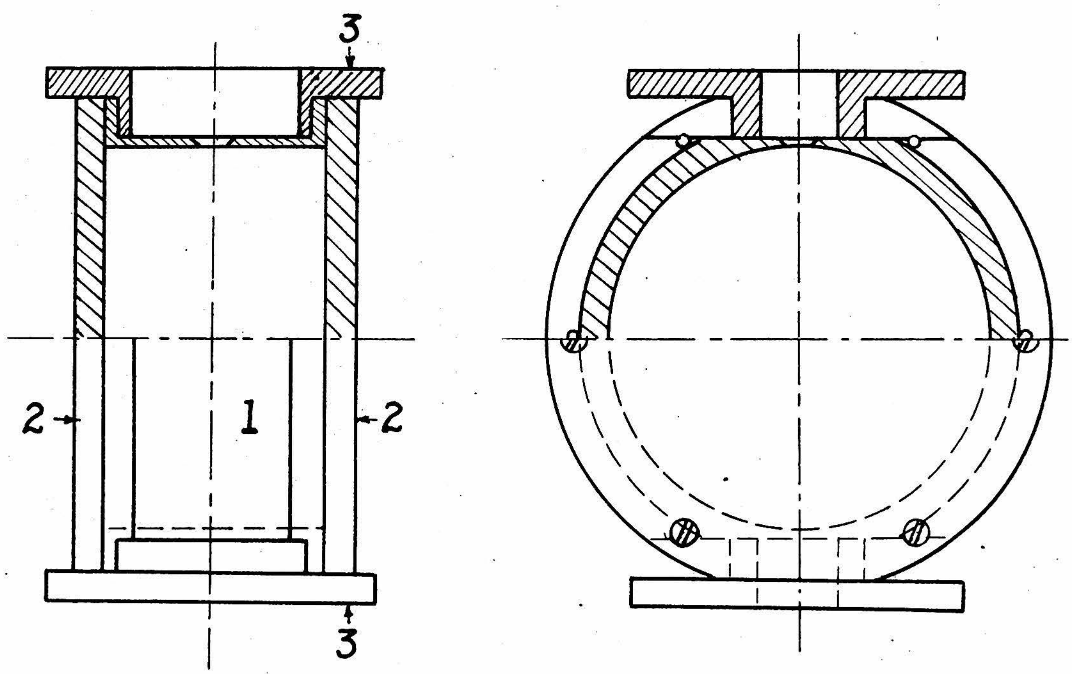

1 main body
2 end plates
3 wave guide flanges

Fig. 4. Cavity assembly drawing.

for which rigorous solutions are available (see part V).

The cavity was copper plated and then silver plated to increase the Q. The plating was probably not more than 0.0002 inches thick but this is sufficient since the skin depth for silver at 8910 megacycles is only 2.7×10^{-5} inches. This was confirmed by the measurements of Q values before and after silvering (see part VI).

3. Volume Measuring Apparatus

A number of methods for measuring the cavity volume were tried. It was found that it is not too easy to fill the cavity completely with distilled water. Because of the comparatively large weight of the cavity itself (about 500 grams), it was not possible to determine the internal volume by weighing the cavity empty and filled with water. The cavity had to be filled from a light container which could be weighed, before and after, on available chemical balances.

The method finally adopted is illustrated on Figs. 5 to 7. A capillary glass tube had one end drawn out into a fine tip. The other end was ground flat and waxed into a brass sleeve which, in turn, was bolted to one of the wave guide flanges of the cavity. A plug bolted to the second wave guide flange served to close the other coupling iris. A side arm was joined to the glass capillary with a three-way stop cock at the junction. The side arm could be connected to an aspirator or a vacuum pump.

With the three-way cock in position 1 (see Fig.7), distilled water was drawn up from a flask with the aid of

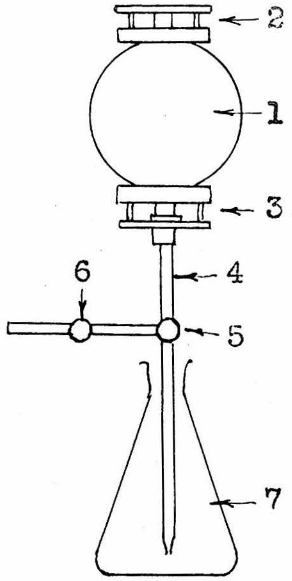

1 Cavity

2 Plug for coupling iris bolted to wave guide flange

3 Waxed-in sleeve on capillary bolted to wave guide flange

4 Glass capillary tube

5 Three-way stop cock

6 Two-way stop cock

7 Flask with distilled water

Fig. 5. Volume measuring assembly.

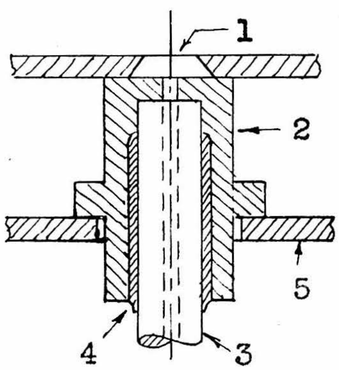

1 Coupling iris

2 Brass sleeve

3 Capillary tube

4 Wax seal

5 Plate bolted to wave guide flange

Fig. 6. Detail of waxed-in sleeve.

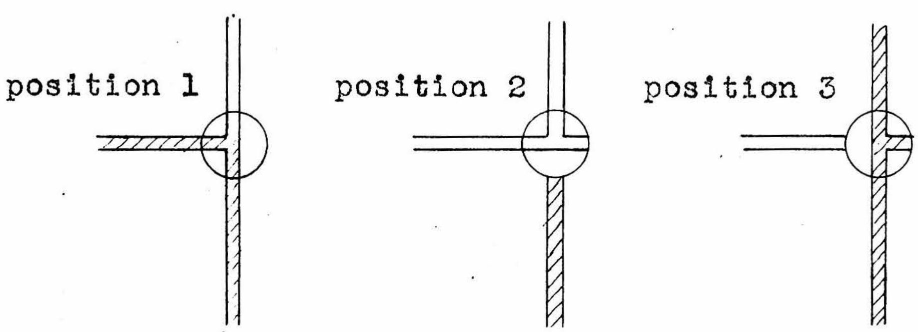

Fig. 7. Switching cycle for three-way cock.

an aspirator. When the water completely filled the bottom part of the capillary up to the cock, the latter was turned to position 2. The aspirator then suctioned off the excess water. Finally, a vacuum pump was connected to the side arm through a drying tube and the cavity and adjoining tubing were evacuated. The water flask was then replaced by another bottle containing distilled water which had been carefully weighed. When the cock was turned to position 3, water was forced up into the cavity by the outside atmospheric pressure. The bottle was then weighed again and the reduction in weight was determined. To correct for the volume in the passages of the stop cock and the short section of tubing between cock and cavity, the above procedure was repeated without the cavity, but with the end of the capillary sealed off.

Although the three-way cock was properly greased, it was found that a thin film of water would form around the passages when the cock was turned from position 2 to position 3. This was probably due to slight wear in the center portion of the cock. The vacuum pump was therefore still connected to the weighing bottle through a fine leak and results of the volume measurement were not too consistent and could not be relied upon. This difficulty was overcome by placing another stop cock in the side arm of the capillary. This cock was closed before turning the first cock to position 3. Water was then also forced into the short connecting capillary between the cocks. This added a little to the volume but considerably improved the consistency of the results.

V. Analysis of the Cavity Excitation Problem

1. Expansion in Normal Modes.

The steady-state fields in a charge-free cavity of volume V, enclosed by a perfectly conducting surface S, can be derived from a single vector potential $\check{\underline{A}}$ which has zero divergence and satisfies the wave equation

$$\nabla\times(\nabla\times\check{\underline{A}}) - \beta^2\check{\underline{A}} = 0 \tag{5.1}$$

where

$$\beta = \omega\sqrt{\mu\varepsilon}$$

The boundary conditions restrict the allowable values for β to a discrete set of eigennumbers, and the corresponding eigenfunctions of $\check{\underline{A}}$ are the normal modes of oscillation of the cavity. The latter satisfy the orthogonality relations

$$\int_V \check{\underline{A}}_a\cdot\check{\underline{A}}_b\,dv = 0 \quad (unless \quad a = b) \tag{5.2}$$

where a and b designate any two normal modes. Any field $\check{\underline{A}}$ inside the cavity can be expanded in terms of these orthogonal vector functions provided that $\check{\underline{A}}$ is normal to the cavity boundary, or normal to a portion of this boundary and tangential to the rest (20).

Following Condon (21), it is convenient to write

$$\check{\underline{A}} = \sum_a \check{\underline{A}}_a = \sum_a \check{p}_a\underline{A}_a^o \tag{5.3}$$

where $\check{p}_a$ represents the complex amplitude of the ath mode and the $\underline{A}_a^o$ are normalized potentials such that

$$\int_V \underline{A}_a^o\cdot\underline{A}_b^o\,dv = \delta_a^b V \tag{5.4}$$

It is evident that the electric and magnetic fields can be expanded in a similar fashion. The amplitude coefficients will be identical with those for the vector potential if we define normalized fields by the relations

$$\check{\underline{E}}_a^o = -j\omega \underline{A}_a^o \tag{5.5}$$

$$\underline{B}_a^o = \nabla \times \underline{A}_a^o \tag{5.6}$$

These fields then satisfy the orthogonality relations

$$\int_V \check{\underline{E}}_a^o \cdot \hat{\underline{E}}_a^o \, dv = \omega_a^2 V \tag{5.7}$$

$$\int_V \underline{B}_a^o \cdot \underline{B}_a^o \, dv = \beta_a^2 V \tag{5.8}$$

For the TE_{011} mode in a circular cylindrical cavity of radius R (diameter D) and length L the normalized potential and the normalized fields can be shown to be

$$\underline{A}_a^o = \underline{a}_\varphi \sqrt{2} \, \frac{J_1(k_{01} r)}{J_0(k_{01} R)} \sin \frac{\pi z}{L} \tag{5.9}$$

$$\check{\underline{E}}_a^o = -\underline{a}_\varphi \, j\omega \sqrt{2} \, \frac{J_1(k_{01} r)}{J_0(k_{01} R)} \sin \frac{\pi z}{L} \tag{5.10}$$

$$\underline{B}_a^o = -\frac{\sqrt{2}}{J_0(k_{01} R)} \left\{ \underline{a}_r \frac{\pi}{L} J_1(k_{01} r) \cos \frac{\pi z}{L} + \underline{a}_z \, k_{01} J_0(k_{01} r) \sin \frac{\pi z}{L} \right\} \tag{5.11}$$

where k_{01} is given by

$$J_0'(k_{01} R) = 0 \quad [\text{or } J_1(k_{01} R) = 0]$$

and hence

$$k_{01} R = r_{01} = 3.8317060$$

2. Effect of Finite Conductivity of Cavity Walls

In an actual metal cavity the walls are not perfectly conducting. A small component of electric field will exist tangential to the surface. If the cavity is excited through an iris a tangential electric field will also be present across the hole to satisfy boundary conditions there. Strictly speaking, such a field can no longer be expanded in terms of orthogonal normal modes, but if we are only interested in relations close to a particular resonance mode this can be done approximately. One can assume that the cavity field is not changed, to a first approximation, from that in an ideal cavity. The tangential electric field over the metallic boundary can then be estimated using skin effect formulas and the unperturbed tangential magnetic field at the surface. Similarly, one can obtain the field distributions over the coupling irises in terms of the unperturbed exciting fields either by static methods using Smythe's double current sheets or by the solution of a particular integral equation as pointed out by Bethe. For high Q cavities the perturbed field solutions obtained in this manner will be almost rigorous.

A suitable expression for the amplitude coefficients in (5.3) can be obtained by applying Green's vector identity to the vectors $\check{\underline{A}}$ and $\underline{A}_a^\circ$. Thus

$$\int_V [\underline{A}_a^\circ \cdot \nabla\times(\nabla\times\check{\underline{A}}) - \check{\underline{A}}\cdot\nabla\times(\nabla\times\underline{A}_a^\circ)]dv = \int_S [\check{\underline{A}}\times\nabla\times\underline{A}_a^\circ - \underline{A}_a^\circ\times\nabla\times\check{\underline{A}}]\cdot\underline{n}\,dS \qquad (5.12)$$

Since both $\check{\underline{A}}$ and $\underline{A}_a^\circ$ satisfy the wave equation (5.1) and since the normalized vector potential $\underline{A}_a^\circ$ has no component tangential to the surface S, this reduces to

$$(\beta^2-\beta_a^2)\int_V \check{\underline{A}}\cdot\underline{A}_a^\circ\,dv = \int_S \check{\underline{A}}\times\underline{B}_a^\circ\cdot\underline{n}\,dS = -\frac{1}{j\omega}\int_S \underline{n}\times\check{\underline{E}}\cdot\underline{B}_a^\circ\,dS$$

or by (5.3) and (5.4) to

$$(\beta^2-\beta_a^2)\,\check{p}_a = -\frac{1}{j\omega V}\int_S \underline{n}\times\check{\underline{E}}\cdot\underline{B}_a^\circ\,dS. \qquad (5.13)$$

The surface integral on the right can be split into three integrals over portions of the surface:

(a) the metallic portion excluding the irises (S_0),

(b) the input iris (S_1),

(c) the output iris (S_2).

Only the first part will be dealt with here and the irises will be treated in later sections.

In evaluating the integral over the metallic portion of the boundary very little error is introduced by extending the integral over the total cavity surface disregarding the irises entirely. Provided that the skin depth δ is small compared to the radius of curvature of the cavity walls, one obtains from the skin effect formulas (22) the following relation between linear current density and tangential electric field:

$$\check{\underline{J}} = \frac{\sigma\delta}{1+j}\check{\underline{E}}_t$$

Since $\underline{n}$ in equations (5.12) and (5.13) is defined as the unit outward normal to the surface S one gets

$$\underline{n}\times\check{\underline{E}} = \frac{1+j}{\sigma\delta}\,\underline{n}\times\check{\underline{J}} = \frac{1+j}{\sigma\delta}\check{\underline{H}} = \frac{1+j}{\sigma\delta}\sum_a \check{p}_a\,\underline{H}_a^o .$$

Close to the resonance frequency of a given mode only one term in the above summation will be of importance and further off resonance all terms will be negligible. Hence only one term need be retained and

$$\underline{n}\times\check{\underline{E}} \cong \frac{1+j}{\sigma\delta}\check{p}_a\,\underline{H}_a^o \quad \text{on } S . \tag{5.14}$$

Therefore

$$\frac{1}{j\omega V}\int_{S_0}\underline{n}\times\check{\underline{E}}\cdot\underline{B}_a^o\,dS = -\frac{1-j}{\sigma\delta\omega\mu V}\check{p}_a\int_S \underline{B}_a^o\cdot\underline{B}_a^o\,dS = -\frac{1-j}{Q_a}\beta_a^2\,\check{p}_a$$

where Q_a is the unloaded cavity Q for the a th mode as usually defined:

$$\frac{1}{Q_a} = \frac{\int_S \underline{B}_a^o\cdot\underline{B}_a^o\,dS}{\omega_a\sigma\delta\mu\int_V \underline{B}_a^o\cdot\underline{B}_a^o\,dv} = \frac{\int_S \underline{B}_a^o\cdot\underline{B}_a^o\,dS}{\omega_a\mu\sigma\delta\beta_a^2 V} \tag{5.15}$$

Equation (5.13) now becomes

$$\left(\beta^2-\beta_a^2+\frac{1-j}{Q_a}\beta_a^2\right)\check{p}_a = -\frac{1}{j\omega V}\int_{S_1S_2}\underline{n}\times\check{\underline{E}}\cdot\underline{B}_a^o\,dS \tag{5.16}$$

It is seen that resonance occurs now when

$$\beta^2-\beta_a^2+\frac{1}{Q_a}\beta_a^2 = 0$$

or

$$\beta \cong \beta_a\left(1-\frac{1}{2Q_a}\right)$$

provided that Q_a is large enough. In that case, Q is a measure of the band width at resonance. The fractional shift in resonance frequency due to the finite conductivity of the walls is thus

$$\frac{\Delta f}{f} = \frac{\Delta\beta}{\beta_a} = -\frac{1}{2Q_a} . \tag{5.17}$$

For the TE_{011} mode and the adopted cavity dimensions

$$Q_a = \frac{30\pi^2 (3)^{3/2}}{R_s(1+2\rho_0)} = \frac{713}{R_s} . \tag{5.18}$$

3. Effect of Small Deformations

Although it has been shown in a previous section that no extreme tolerances need be maintained for the length-todiameter ratio of the cavity, it is still necessary to investigate the effect of imperfections in the cavity shape on the resonance frequency. Intuitively, we may expect this effect to be negligible, because when measuring the cavity volume we actually determine a mean linear dimension and effects from positive and negative deviations from the ideal shape will tend to cancel each other.

Bernier and others have calculated the shift in resonance frequency of a cavity due to small deformations by perturbation methods and from general thermodynamic principles(23). Their result can be obtained directly from equation (5.13). Since small deformations, finite conductivity of boundaries, and coupling holes affect the resonance frequency only slightly, it is permissible to calculate the three effects separately. In the following we will therefore disregard the coupling holes and assume perfectly conducting walls.

Let us assume that the electric and magnetic fields are known in the cavity volume bounded by the surface S (Fig.8). If the boundary is slightly deformed to a neighboring surface S', the fields will be changed somewhat and the resonance frequency may be expected to shift.

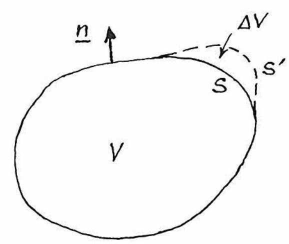

Fig.8. Deformation of cavity.

The electric field is now everywhere normal to the surface S', but not necessarily normal to S. The surface integral in (5.13) will therefore, in general, be different from zero. It can be changed into a more convenient form by applying Gauss's theorem to the vector $\check{\underline{E}} \times \underline{B}_a^o$ in the volume increment ΔV between the surfaces S and S':

$$\int_{\Delta V} \nabla\cdot(\check{\underline{E}}\times\underline{B}_a^o)\,dv = -\int_S \check{\underline{E}}\times\underline{B}_a^o\cdot\underline{n}\,dS + \int_{S'} \check{\underline{E}}\times\underline{B}_a^o\cdot\underline{n}\,dS$$

The negative sign in the first surface integral must be chosen because $\underline{n}$ was defined to be the outward-pointing normal to the cavity volume V and hence represents the inward-pointing normal to ΔV which is taken to be positive for a volume increase. The second surface integral above vanishes because, by hypothesis, $\check{\underline{E}}$ is normal to the surface S'. Hence, the right-hand side of (5.13) becomes

$$-\frac{1}{j\omega V}\int_S \underline{n}\times\check{\underline{E}}\cdot\underline{B}_a^o\,dS = +\frac{1}{j\omega V}\int_S \underline{B}_a^o\times\check{\underline{E}}\cdot\underline{n}\,dS = \frac{1}{j\omega V}\int_{\Delta V}\nabla\cdot(\check{\underline{E}}\times\underline{B}_a^o)\,dv .$$

Using the vector identity

$$\nabla\cdot(\check{\underline{E}}\times\underline{B}_a^o) = \underline{B}_a^o\cdot\nabla\times\check{\underline{E}} - \check{\underline{E}}\cdot\nabla\times\underline{B}_a^o$$

and Maxwell's curl equations, the above expression reduces to

$$-\frac{\mu}{V}\int_{\Delta V}\left(\frac{1}{\mu}\check{\underline{B}}\cdot\underline{B}_a^o + \varepsilon\check{\underline{E}}\cdot\check{\underline{E}}_a^o\right)dv$$

Near resonance one may write $\check{\underline{B}} = \check{p}_a\underline{B}_a^o$, $\check{\underline{E}} = \check{p}_a\check{\underline{E}}_a^o$, and noting the 90^o phase difference between $\check{\underline{E}}_a^o$ and $\underline{B}_a^o$ from (5.5) and (5.6) one obtains finally

$$-\check{p}_a\frac{\mu}{V}\int_{\Delta V}\left[\frac{1}{\mu}(B_a^o)^2 - \varepsilon(E_a^o)^2\right]dv$$

or, making use of (5.8),

$$-\check{p}_a\beta_a^2\,\frac{\int_{\Delta V}\left[\frac{1}{2\mu}|B_a^o|^2 - \frac{\varepsilon}{2}|E_a^o|^2\right]dv}{\int_V\frac{1}{2\mu}|B_a^o|^2\,dv}\,.$$

When this expression is substituted into equation (5.13) it is seen to give rise to a frequency shift

$$\frac{\Delta f}{f} = \frac{\Delta\beta}{\beta_a} = -\frac{1}{2}\,\frac{\int_{\Delta V}\left[\frac{1}{2\mu}B^2 - \frac{\varepsilon}{2}E^2\right]dv}{\int_V\frac{1}{2\mu}B^2\,dv}\,. \qquad (5.19)$$

Subscripts have been dropped as irrelevant.

An examination of equation (5.19) shows that the fractional change in resonance frequency is proportional to the fractional changes in the average electric and magnetic energies stored in the cavity volume. The resonance frequency may be increased or decreased by the same deformation of the boundary surface depending on whether the deformation occurs in a region of high electric or high magnetic field.

It is interesting to note that (5.19) could also have been obtained from a lumped-circuit analogy. For a resonant L-C cicuit

$$f = \frac{1}{2\pi\sqrt{LC}}$$

and hence

$$\frac{\Delta f}{f} = -\frac{1}{2}\left(\frac{\Delta L}{L} + \frac{\Delta C}{C}\right)$$

The stored electric and magnetic energies are, respectively,

$$U_E = \frac{1}{2} C V^2 \quad or \quad U_E = \frac{1}{2}\frac{Q^2}{C} = \frac{1}{2}\frac{I^2}{\omega^2 C}$$

$$U_M = \frac{1}{2} L I^2$$

and hence

$$\frac{\Delta f}{f} = -\frac{1}{2}\left(\frac{\Delta U_M}{U_M} \pm \frac{\Delta U_E}{U_E}\right) \tag{5.20}$$

The ambiguity in sign arises because of the two expressions for U_E. Evidently, we must use the second expression for U_E ("constant-current analogy") in our problem to obtain the lower sign in (5.20). Other problems may require the use of the first expression for U_E ("constant-voltage analogy") and the upper sign in (5.20). This will be the case, for instance, if the cavity volume is not changed but a small amount of dielectric is introduced into the cavity.

Equation (5.19) must now be applied to the following imperfections in the shape of a circular cylindrical cavity:

(a) ellipticity in the cavity body,

(b) tilted end plates, and

(c) random dents in the cavity walls.

The first two points can be dealt with very briefly. Any deformation of the cross-section of the cavity over its entire length can be represented by expressing the equation of the cylindrical wall in terms of a Fourier series

$$r = R\left\{1 + \sum_n (\alpha_n \cos n\varphi + \beta_n \sin n\varphi)\right\} \tag{5.21}$$

Similarly, a tilt in the end plates can be written as

$$z = L\,(1 + \alpha \cos n\varphi) \tag{5.22}$$

The α's and β's are infinitesimals and hence the above deformations leave the volume of the cavity unchanged to a first approximation.

For the TE_{011} mode in a cylindrical cavity no electric field exists near the surface and the second term in (5.19) will vanish. The first term of that equation is also equal to zero because the magnetic field is axially symmetric and the net volume change is zero for both types of deformation.

There remains to be analysed the question of random dents. Because of the axial symmetry of the fields it will be sufficient to estimate the effect of circular grooves either in the end plates or the main cavity body. Such grooves may actually occur as a result of the machining process in the lathe. To get an upper limit for the frequency shift to be expected we must place the grooves in regions of maximum magnetic field, i.e. half-way between the end plates on the cylindrical surface and at a distance R_1 from the axis on the end plates given by $J_1(k_{01}R_1) = 0.58$ (maximum value of J_1).

To keep the volume unchanged it is, of course, necessary to recess the rest of the cavity surface as shown in Fig. 9. If the width of the grooves is b and their depth is h, the recesses for the cylindrical surface and the end surfaces are, respectively,

$$h' = \frac{b}{L-b}\,h \cong \frac{b}{L}\,h \tag{5.23}$$

and

$$h' = \frac{2\pi R_1 b}{\pi R^2 - 2\pi R_1 b}\,h \cong \frac{2R_1 b}{R^2}\,h\,. \tag{5.24}$$

Equation (5.19) can now be evaluated for the two cases using (5.8),(11),(23), and (24). For the groove in the cylindrical wall one obtains for the residual frequency shift approximately

$$\frac{\Delta f}{f} \cong -\frac{\pi R h b}{V}\left(\frac{k_{01}}{\beta}\right)^2 \tag{5.25}$$

and for the grooves in the end plates

$$\frac{\Delta f}{f} \cong -\frac{2\pi R_1 b h}{V}\left(\frac{\pi}{\beta L}\right)^2\left\{\frac{J_1^2(k_{01}R_1)}{J_0^2(k_{01}R)} - 1\right\} \tag{5.26}$$

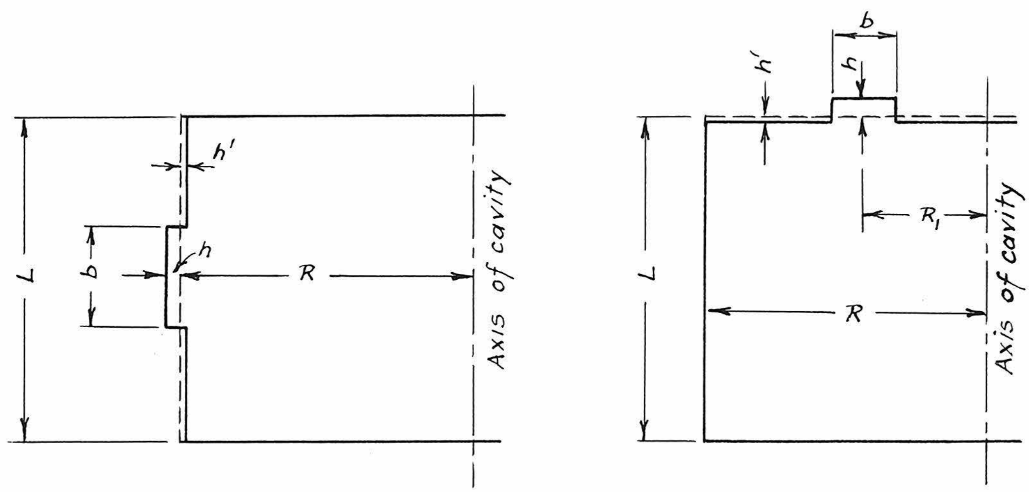

Fig. 9. Grooves in the cavity surface.

These expressions can be further simplified by using the particular cavity dimensions adopted previously. From equations (3.11) and (3.13) we have

$$\left(\frac{k_{01}}{\beta_a}\right)^2 = \left(\frac{k_{01}\lambda}{2\pi}\right)^2 = \left(\frac{r_{01}\lambda}{\pi D}\right)^2 = \frac{2}{3} \tag{5.27}$$

and

$$\left(\frac{\pi}{\beta_a L}\right)^2 = \left(\frac{\lambda}{2L}\right)^2 = \frac{1}{3} \tag{5.28}$$

Furthermore, R_1 was chosen to make $J_1(k_{01}R_1) = 0.58$, and $J_0(k_{01}R) = -0.40$ because $J_1(k_{01}R) = 0$. Hence (5.25) and (5.26) become, respectively,

$$\frac{\Delta f}{f} \cong -\frac{1}{3}\,\frac{2\pi R b h}{V} \tag{5.29}$$

$$\frac{\Delta f}{f} \cong -\frac{1}{3}\,\frac{2\pi R_1 b h}{V} \tag{5.30}$$

When substituting numerical values into these equations, it will be seen that grooves and dents may have considerable effect on the resonance frequency (at least, compared to the desired precision) unless construction tolerances are kept to a few tenthousandths of an inch. It must be noted, however, that the above derivation assumed the worst possible case which is extremely unlikely. In a well-machined cavity grooves will be more uniformly distributed, and the residual frequency shift will thereby be substantially reduced.

4. Effect of Thin Coupling Irises

Both input and output iris will shift the resonance frequency and cause a lowering of the effective cavity Q and hence, and increase in the bandwidth at resonance (24,25). These effects can again be estimated from equation (5.13) if reasonable assumptions can be made as to the tangential electric field within the irises. This is possible for irises small compared to the wavelength by using static field solutions for a hole in an infinite, plane sheet and Smythe's double current sheet method (26) or by using a method introduced by Bethe (27). The former method will be used here.

Let us first consider the output iris and assume that, to a first approximation, the iris can be represented by a circular hole of radius c in a very thin, plane metal sheet (Fig. 10). We wish to find the perturbation of the field near the hole when the sheet forms the boundary of a uniform magnetic field of induction B_0 parallel to the sheet. Such a field must be derivable from a scalar magnetostatic potential and is best expressed in terms of oblate spheroidal harmonics (28).

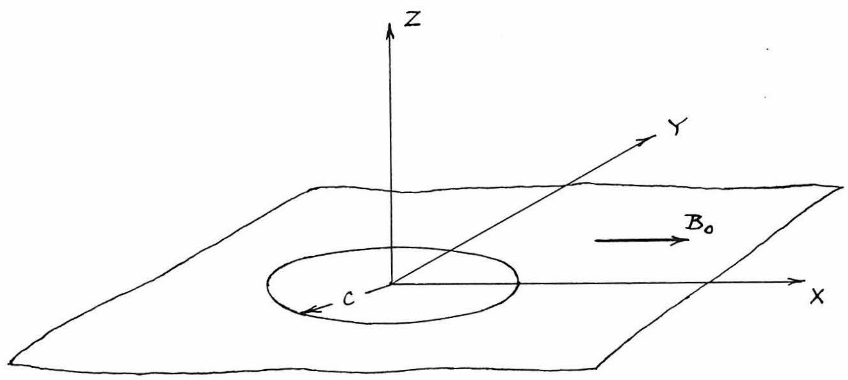

Fig.10. Circular iris in thin sheet.

W.R. Smythe has shown that a suitable potential is

$$\mu\Omega = B_0 c\left[j P_1^1(j\zeta) + \frac{1}{\pi} Q_1^1(j\xi)\right] P_1^1(\xi)\cos\varphi$$
$$= -B_0 x\left[1 - \frac{1}{\pi}\left(\cot^{-1}\xi - \frac{\xi}{1+\xi^2}\right)\right] \qquad (5.31)$$

where x is the rectangular coordinate of the point (ξ, ζ, φ) measured in the direction of B_0 from the center of the hole given by

$$x = \rho\cos\varphi = c(1-\xi^2)^{1/2}(1+\xi^2)^{1/2}\cos\varphi \qquad (5.32)$$

Hence the first term in (5.31) represents a uniform field B_0

on both sides of the sheet, while the second term has the effect of wiping out the field below the sheet for large negative values of ζ but only slightly affects the field above the sheet.

The normal B in the hole is

$$B_z = -\frac{\mu}{h_2}\frac{\partial\Omega}{\partial\zeta}\Big|_{\zeta=0} = \frac{2B_0 x}{\pi(c^2-\rho^2)^{1/2}} \tag{5.33}$$

and from a consideration of flux linkages in the double current sheet the tangential electric field is

$$E_y = -j\omega\int B_x\, dx = +\frac{2j\omega B_0}{\pi}(c^2-\rho^2)^{1/2}$$

or

$$\underline{n}\times\check{\underline{E}} = \frac{2j\omega}{\pi}\check{\underline{B}}_0(c^2-\rho^2)^{1/2} \tag{5.34}$$

We shall assume that energy emitted through the output iris into the waveguide beyond is completely absorbed and not reflected back into the cavity. This will certainly be the case if the detector crystal is reasonably well matched into the guide and if an attenuator is placed between cavity and crystal. Then we may take the unperturbed cavity field at the hole for the exciting field $\check{\underline{B}}_0$. Since the hole is small this may be assumed to be constant in the vicinity of the iris and equal to the unperturbed field at the center of the hole:

$$\check{\underline{B}}_0 = \check{\underline{B}}_a(0) = \check{p}_\alpha \underline{B}_a^0(0)$$

The right side of (5.13) then becomes (for the output iris only)

$$-\frac{1}{j\omega V}\underline{B}_a^0(0)\cdot\int_{S_2}\underline{n}\times\check{\underline{E}}\, dS = \frac{2}{\pi V}\check{p}_a[B_a^0(0)]^2\int_0^c 2\pi\rho(c^2-\rho^2)^{1/2}d\rho = \frac{4}{3}c^3\frac{\check{p}_a}{V}[B_a^0(0)]^2$$

From (5.11) and (27)

$$[B_a^0(0)]^2 = 2k_{01}^2 = \frac{4}{3}\beta_a^2 \tag{5.35}$$

If this is put into the above expression one obtains

$$\frac{16}{9}\,\frac{c^3}{V}\,\check{p}_a\,\beta_a^2$$

When substituted in equation (5.13) this corresponds to a frequency shift

$$\frac{\Delta f}{f} = \frac{\Delta\beta}{\beta} = -\frac{8}{9}\,\frac{c^3}{V} = -\frac{2}{3}\,\frac{M}{V} \qquad (5.36)$$

where

$$M = \frac{4}{3}c^3 \qquad (5.37)$$

is Bethe's magnetic polarizability of the iris.

We must find the energy radiated into the output guide to find the effect of the iris on the cavity Q. This can be done by expanding the transverse electric field in the guide in a series of orthogonal normal modes (29) and matching to the assumed field in the plane of the iris (see Fig. 11):

$$\begin{aligned} E_y\Big|_{z=0} &= \frac{2j\omega}{\pi}\,B_a(0)\,(c^2-\rho^2)^{1/2} && \text{for } \rho < c \\ &= 0 && \text{for } \rho > c \end{aligned} \qquad (5.38)$$

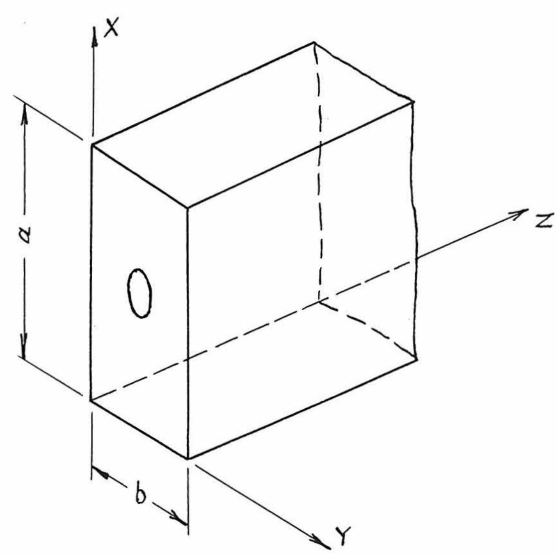

Fig. 11. Coupling to output wave guide.

Since only the TE_{10} mode is propagated in the guide, it is sufficient to calculate the amplitude for this mode. The field expressions for this mode at $z = 0$ are

$$\check{\underline{E}}_2 = \underline{j}\, \check{C}_2 \sin \frac{\pi x}{a} \triangleq \check{C}_2 \underline{E}_{10} \tag{5.39}$$

$$\check{\underline{H}}_2 = \underline{i}\, \frac{\lambda}{\lambda_g \eta}\, \check{C}_2 \sin \frac{\pi x}{a} \triangleq \check{C}_2 \underline{H}_{10}\,. \tag{5.40}$$

Making use of the orthognality properties of the transverse field components one obtains

$$\check{C}_2 = \frac{\int_0^a \int_0^b \check{\underline{E}}_2 \big|_{z=0} \cdot \underline{E}_{10}\, dx\,dy}{\int_0^a \int_0^b \underline{E}_{10} \cdot \underline{E}_{10}\, dx\,dy} = \frac{4 j\omega\, \check{B}_a(0) \int_0^c \rho\,(c^2-\rho^2)^{1/2}\, d\rho}{\frac{1}{2}ab}$$

$$= \frac{8c^3}{3ab}\, j\omega\, \check{B}_a(0) = \frac{2j\omega M\, \check{B}_a(0)}{ab}\,. \tag{5.41}$$

The power transmitted into the output wave guide through the iris can be calculated from (5.39),(40) and (41):

$$P_2 = \frac{1}{2}\int_0^a \int_0^b \check{E}_2\, \hat{H}_2\, dx\,dy = \frac{4\pi^2 \eta M^2}{ab\lambda\lambda_g} \left[\frac{B_a(0)}{\mu}\right]^2. \tag{5.42}$$

It is seen to be proportional to the sixth power of the iris radius. The power loss in the cavity walls due to finite conductivity is $P_L = \frac{\pi}{8} R_s D^2 (1 + 2\rho_0) \left[\frac{B_a(0)}{\mu}\right]^2$ (5.43)

and hence the ratio

$$\frac{P_2}{P_L} = \frac{32\pi M^2}{ab\lambda\lambda_g D^2}\, \frac{\eta}{R_s}\, \frac{1}{1+2\rho_0}\,. \tag{5.44}$$

With numerical values substituted (see part VI) this ratio becomes .042. Hence the bandwidth at resonance is increased 4.2% due to the output window , and the cavity Q is decreased by approximately the same amount.

The ratio of the magnetic field in the principal wave guide mode to the undisturbed cavity field at the iris is from (5.39) and (40)

$$\frac{4\pi M}{ab\lambda_g}$$

When substituting numerical values this becomes .008.

Hence the field in the principal wave guide mode just outside the iris is less than 1% of the unperturbed cavity field just inside the window. This justifies the original assumption that the exciting field outside the cavity may be neglected.

Similar relations may be obtained for the input iris. Here, of course, we must consider the field incident from the input wave guide. It is not negligible with respect to the cavity field and represents the forcing function in equation (5.13) in terms of which the amplitude of oscillation in the cavity can be calculated. Analogous to equations (5.39) and (5.40), we take the incident wave guide fields to be

$$\check{\underline{E}}_1 = \check{C}_1 \underline{E}_{10} \tag{5.45}$$

$$\check{\underline{H}}_1 = \check{C}_1 \underline{H}_{10} \tag{5.46}$$

To a first approximation we may assume that almost the entire incident energy is reflected at the end of the guide containing the iris. It will be shown later in this section that only a minute fraction of the incident power is transmitted through the cavity. The effective exciting field on the inside of the iris will therefore be

$$\check{B}_0 = \check{B}_a(0) - 2\check{B}_1(0) = \check{p}_a B_a^0(0) - 2\check{B}_1(0) \tag{5.47}$$

The first term is identical with the exciting field at the output iris and will lead to an identical frequency shift and to the same contribution to the loaded band width of the cavity. The second term contributes to the surface integral in (5.13) an amount: $-\frac{2M}{V}\check{B}_1(0)\, B_a^0(0)$.

When account is taken of all the perturbations discussed in this and previous sections, the amplitude of oscillation in the cavity will be given by

$$\left(\beta^2 - \beta_a'^2 - j\frac{\beta_a^2}{Q_a'}\right)\check{p}_a = -\frac{2M}{V}B_a^o(0)\check{B}_1(0) \tag{5.48}$$

where the actual resonance frequency is

$$\beta_a' = \beta_a\left(1 - \frac{1}{2Q_a} - \frac{4}{3}\frac{M}{V}\right) \tag{5,49}$$

and the loaded Q is given by

$$\frac{1}{Q_a'} = \frac{1}{Q_a} + \frac{2}{Q_i} = \frac{1}{Q_a}\left(1 + 2\frac{P_2}{P_L}\right). \tag{5.50}$$

Here $1/Q_i$ is the additional band width contributed by each of the two irises.

At resonance

$$(p_a)_{res} = \frac{2M}{\beta_a^2 V}B_a^o(0)B_1(0)Q_a'$$

and the cavity field becomes, making use of (5.35) and (46),

$$B_a(0) = \frac{8}{3}\frac{MQ_a'}{V}B_1(0). \tag{5.51}$$

Numerical substitution shows that the cavity field at the iris is about ten times as large as the incident field. The principal field in the output wave guide was shown to be only 0.8% of the unperturbed cavity field at the iris. It is therefore about 8% of the incident field in the input guide. Approximately 0.64% of the incident power is transmitted through the cavity and hence from (5.44) about 16% of the incident power enters the cavity at the input iris, 84% being reflected there. The reflected field is thus 92% of the incident field and only 4% error was introduced in (5.47) by assuming the reflected field equal to the incident field.

5. Effect of Thick Coupling Irises

The representation of the irises by holes in very thin sheets is, of course, only a very rough approximation. The actual coupling holes were about one millimeter deep and counterbored with a half-angle of 41° (see Fig. 12). Since the experimentally determined frequency shift due to these coupling holes (see part VI) turned out to be only about two-thirds that predicted from the thin-sheet formulas, this case had to be investigated more thoroughly. This can be done by a method suggested by W.R. Smythe (30).

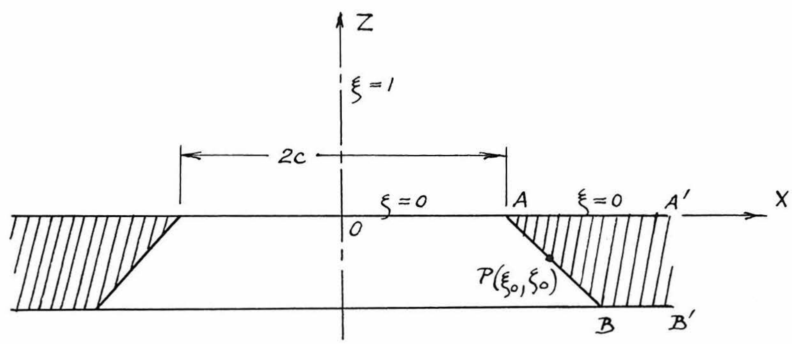

Fig. 12. Thick coupling iris.

The potential of (5.31) may be generalized to

$$\mu\Omega = B_0 c\left[j P_1^1(j\zeta) P_1^1(\xi) + \sum_{n\ odd} A_n Q_n^1(j\zeta) P_n^1(\xi)\right]\cos\varphi \qquad (5.52)$$
$$= -B_0 x + B_0 c \cos\varphi \sum_{n\ odd} A_n Q_n^1(j\zeta) P_n^1(\xi)$$

The above expression represents a possible solution of Laplace's equation in oblate spheroidal coordinates. The choice of odd values of n is dictated by the fact that the $Q_n^1(j\zeta)$ with odd n go to infinity as ζ goes to $-\infty$, but vanish as ζ goes to $+\infty$. Just the opposite is the case for even subscripts n. The above solution automatically makes A-A′ a line of force and A-B-B′ may be made a line of force by proper choice of coefficients. This can be accomplished by choosing a number of points along the boundary of the hole. The condition that the same line of force passes through each of the points is given by a linear algebraic equation. The set of equations obtained in this manner can be solved for the coefficients A_n.

Let ξ_0, ζ_0 be the coordinates of a point P on the boundary of the hole (see Fig. 12). It is easily seen that the condition that P lies on the surface of the same tube of force as A-A$'$ is the vanishing of the total normal flux through the surface $\zeta = \zeta_0$ between $\xi = 0$ and $\xi = \xi_0$, and between $\varphi = -\frac{\pi}{2}$ and $\varphi = +\frac{\pi}{2}$, that is

$$\int_{-\frac{\pi}{2}}^{+\frac{\pi}{2}} \int_0^{\xi_0} \left[\frac{1}{h_2} \frac{\partial(\mu\Omega)}{\partial\zeta} h_1 h_3 \right]_{\zeta_0} d\xi \, d\varphi = 0.$$

Since for oblate spheroidal coordinates (28)

$$h_1 = c\left(\frac{\xi^2 + \zeta^2}{1 - \xi^2}\right)^{1/2} \qquad (5.53)$$

$$h_2 = c\left(\frac{\xi^2 + \zeta^2}{1 + \zeta^2}\right)^{1/2} \qquad (5.54)$$

$$h_3 = c\,(1 + \zeta^2)^{1/2}(1 - \xi^2)^{1/2}, \qquad (5.55)$$

the above condition reduces to

$$\int_0^{\xi_0} \left.\frac{\partial\Omega}{\partial\zeta}\right|_{\zeta_0} d\xi = 0$$

or

$$j \frac{d}{d\zeta_0} P_1^1(j\zeta_0) \int_0^{\xi_0} P_1^1(\xi)\, d\xi + \sum_{n\ odd} A_n \frac{d}{d\zeta_0} Q_n^1(j\zeta_0) \int_0^{\xi_0} P_n^1(\xi)\, d\xi = 0 \qquad (5.56)$$

We can solve for a finite number of coefficients A_n if we write this equation for an equal number of points on the boundary A-B. The result will, of course, fit the boundary only approximately over a finite region, but the approximation can be made extremely good by choosing points close to the edge A. The reason for this is, that we are only interested in the fields in the plane of the hole ($\zeta = 0$), and that the shape of the boundary at larger distances from the hole is of no importance because the fields drop off very rapidly for negative values of ζ.

The result of a calculation for a circular hole tapered at 45° using four points (see Appendix B), is given in the following table. For comparison, the table also contains the result previously quoted for a circular hole in a thin sheet (half-angle of cone 90°), and results obtained by W.R. Smythe for a circular cylindrical hole in a very thick plate (half-angle of cone 0°).

A_n in equation (5.52)	2c 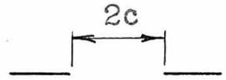	2c 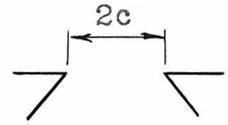	2c 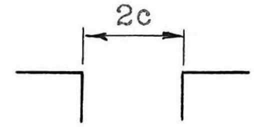
A_1	0.318310	0.2369	0.118295
A_3	0	-0.06042	-0.0256875
A_5	0	0.009305	0.000993431
A_7	0	-0.000741	-0.0000300924
A_9	0		0.000000690751

With the coefficients in (5.52) known, we can proceed, in a manner analogous to that used in the previous section, to find the normal magnetic field and hence the tangential electric field. Since the first term in (5.52) represents a uniform magnetic field parallel to the plane of the hole, it does not contribute anything to the required fields.

Hence, inside the hole

$$B_z = -\frac{\mu}{h_2}\frac{\partial\Omega}{\partial\zeta}\Big|_{\zeta=0} = -B_0 c\cos\varphi\sum_{n\,odd} A_n P_n^1(\xi)\Big[\frac{1}{h_2}\frac{\partial}{\partial\zeta}Q_n^1(j\zeta)\Big]_{\zeta=0} \qquad (5.57)$$

and, since $h_2 = c\xi$ at $\zeta = 0$,

$$E_y = -j\omega\int B_z\,dx = j\omega B_0\sum_n A_n\Big[\frac{\partial}{\partial\zeta}Q_n^1(j\zeta)\Big]_{\zeta=0}\int_0^x \frac{P_n^1(\xi)}{\xi}\cos\varphi\,dx \qquad (5.58)$$

From (5.32) and the definition of $P_n^1(\xi)$ the last equation reduces to

$$E_y = j\omega B_0\sum_{n\,odd} A_n\Big[\frac{\partial}{\partial\zeta}Q_n^1(j\zeta)\Big]_{\zeta=0}\int_0^x \frac{d}{d\xi}P_n(\xi)\,\frac{x\,dx}{\xi} \qquad (5.59)$$

The magnetic polarizability corresponding to (5.37) then becomes

$$\begin{aligned} M &= -\frac{1}{j\omega B_0}\int_{S_2} E_y\,dS \\ &= \sum_{n\,odd} A_n\Big[\frac{\partial}{\partial\zeta}Q_n^1(j\zeta)\Big]_{\zeta=0}\int_0^{2\pi}\int_0^1 \xi\,d\xi\,d\varphi\int_0^x \frac{d}{d\xi}P_n(\xi)\frac{x\,dx}{\xi} \end{aligned} \qquad (5.60)$$

It can be shown (see Appendix C) that the result of the integrations is zero for all terms except the first one. The first term is identical, except for the coefficient, with that previously worked out for the thin sheet case. Hence, one finally obtains

$$M = \frac{2}{3}\pi c^3 A_1\Big[\frac{\partial}{\partial\zeta}Q_1^1(j\zeta)\Big]_{\zeta=0}$$

or, since $\Big[\frac{\partial}{\partial\zeta}Q_1^1(j\zeta)\Big]_{\zeta=0} = 2$ (reference 31),

$$M = \frac{4}{3}c^3\pi A_1 \qquad (5.61)$$

This is seen to reduce to (5.37) for $A_1 = \frac{1}{\pi}$ as it should. The frequency shift due to the irises will only depend on the first coefficient in (5.52), because it is proportional to the polarizability M.

A glance at the above table shows that the frequency shifts for the three types of irises will be approximately in a 3 to 2 to 1 ratio. The shifts decrease with decreasing cone angle. An intuitive consideration of the field penetration into the three irises, could, of course, be used to anticipate such a result.

The relations for power transmission and loaded Q could be revised in a similar manner. This problem is somewhat complicated by the fact that the fields on the wave guide side of the thick irises must also be known. Since exact expressions for the cavity transmission were not required, and since the cavity loading due to the irises was very small anyway, this calculation was not carried out.

VI. Experimental results

1. Preliminary experiments

Before actual measurements of the resonance frequency and the volume of the cavity were undertaken, a number of preliminary experiments were made to check the calibration and performance of the apparatus and to verify some of the relations derived previously. These tests will be discussed in the following order:

(a) Calibration of audio oscillator and i-f receiver.

(b) Checks on performance of multiplier chain.

(c) Loading effects on secondary standard.

(d) Checks on the i-f dots.

(e) Checks on the linearity of the frequency sweep.

(f) Shift of resonance frequency from air to vacuum.

(g) Cavity Q measurements.

(h) Frequency shift due to coupling irises.

(i) Resonance frequency from linear dimensions.

(a) The calibration of the audio oscillator was checked by comparison with the 440-cycle signal from WWV and with the 60-cycle line frequency. Frequency checks were made in steps of 220 cycles up to 1320 cycles and in steps of 30 cycles up to 300 cycles. The i-f receiver was calibrated against an r-f signal generator in the range from 150 to 600 kilocycles. Spot checks were also made using signals from two radio stations at the lower end of the broadcast band.

(b) The proper functioning of the multiplier chain was investigated by measuring the frequency at all its stages. For the lower levels, from 5 to 270 megacycles, a sensitive grid-dip meter was used. At the 2970-megacycle level the wave length could be measured to 1 part in 5000 by means of a coaxial wavemeter. The final stage (8910 megacycles) was checked by a cavity-type wavemeter to about the same accuracy.

(c) The effect of loading on the crystal oscillator was investigated by de-tuning some of the higher frequency stages, and by looking for changes in the audio beat between crystal and WWV. No significant changes could be observed.

(d) A number of obvious tests were made to ascertain that the i-f dots on the oscilloscope were not spurious images, but were actually caused by the heterodyne action between secondary frequency standard and local oscillator: The intensity of the dots changed with variations in either the crystal oscillator or local oscillator power. They disappeared, of course, when either oscillator was switched off. The distance between the dots was proportional to the frequency setting on the i-f receiver. This could be checked fairly accurately by direct measurement on the oscilloscope screen. A rough verification of the above was also possible by observing the change in dial setting on the 3-centimeter wavemeter (see Fig. 1), when the "absorption pip" caused by the meter was moved from one i-f dot to the other. The coincidence between the absorption pip and one of the i-f dots was indicated by a reduction in intensity of that dot.

By turning the tuning dial on the local oscillator, the i-f dots could be brought to the edge of the region of oscillation of the reflex klystron. In this manner, the dots could be made to disappear one after the other, as they crossed over into the zero-output region of the klystron.

(e) As mentioned under (d) above, measurements of i-f dot separation for various intermediate frequencies showed that horizontal beam deflections on the oscilloscope were nearly proportional to frequency increments. This was true over a range of about 2 megacycles. The resonance frequency of a cavity could therefore be measured over a wider frequency range than would have been possible by varying the crystal oscillator frequency alone. It was only necessary to note the position of the resonance peak with respect to the two i-f dots. With the intermediate frequency set at 500 kilocycles (1 megacycle dot separation), and the i-f dots about 1 inch apart on the screen, the resonance peak could be easily located to within 1/20 inch. This corresponds to an accuracy in the frequency determination of better than 1 part in 150,000.

For cavity resonance frequencies differing from the standard frequency by not more than 600 kilocycles, a slight modification of the above method could be used which leads to somewhat higher accuracy. With a suitable setting of the crystal oscillator, the intermediate frequency is varied until one of the i-f dots falls on the resonance peak. The i-f receiver dial then directly indicates the amount by which the resonance frequency differs from the standard.

(f) The actual dimensions of the test cavity differed a little from those originally specified (part IV, 2). It was intended to have the resonance frequency in vacuo close to the crystal standard, but due to the error in construction, the resonance frequency in air fell into that range. The latter could therefore be very accurately measured by the method outlined in part IV. It was then necessary to measure the shift in resonance frequency that occurred when the cavity was evacuated. This could only be done with somewhat lower accuracy by the modification described under (e).

The shift in resonance frequency from air to vacuum amounted to about 2.8 megacycles. The exact value depended on prevailing atmospheric conditions. The shift can also be calculated very accurately from the dielectric constant of air which is given by (32)

$$\varepsilon_r = 1 + \frac{208}{T}\left(P + \frac{4800}{T} P_w\right) 10^{-6} \qquad (6,1)$$

where T = temperature of the air in degrees Kelvin

P = total pressure in mm Hg

P_w = water vapor pressure in mm Hg.

The fractional change in frequency from air to vacuum is

$$\frac{\Delta f}{f} = \frac{1}{2}\frac{\Delta \epsilon}{\epsilon} \cong \frac{104}{T}\left(p + \frac{4800}{T}p_w\right)10^{-6} \qquad (6.2)$$

Values calculated from this formula agreed with experimental results to within 10% or about 0.30 megacycles. This comparatively large discrepancy was mainly due to the non-linearity in the frequency sweep which became quite noticeable for larger frequency deviations.

(g) It was pointed out previously (part II) that the contact resistance between cavity body and end plates does not affect the operation of the cavity for the TE_{011} mode. Hence, calculated Q values should agree very well with measured results if due consideration is given to the loading by the coupling irises. Measurements of the loaded band width at resonance were made before and after the cavity was silvered. A table of comparative results is given below.

	Brass cavity	
	before plating	after plating
Unloaded Q (calculated)	15,100	30,000
Loaded Q (calculated)	14,200	27,600
Band width (calculated)	615 kc	322 kc
Band width (measured)	610 ± 30 kc	320 ± 15 kc

Unloaded Q's were calculated from (5.18), loaded Q's from (5.44) and (5.50). Surface resistances R_s at 8900 megacycles were taken to be 0.0473 and 0.0238 ohms for brass and silver, respectively.

(h) The cavity was originally built with coupling holes 0.120 inches in diameter. The diameters were later enlarged to 0.140 inches to increase the power transmission. The calculated total frequency shifts due to both irises were: 0.97 and 1.54 megacycles, respectively, for the two diameters using the thin sheet formula (5.36), but only 0.72 and 1.15 megacycles using the thick iris formula (5.61). The expected net reduction in resonance frequency after enlarging the holes was therefore:

0.57 megacycles from equations (5.36) and (37), and

0.43 megacycles from equation (5.61)

The measured shift was 0.40 ± 0.05 megacycles. The two measurements were made under almost identical atmospheric conditions. The uncertainty in the measured value arises mainly from the fact that the cavity had to be taken apart to machine the irises. Re-assembling the cavity sometimes led to changes in the resonance frequency of as much as 0.05 megacycles. A similar uncertainty exists in the calculated values. An error of 0.002 inches in the iris diameter corresponds to about 0.05 megacycles in the calculated frequency shift. Within the limits of experimental error the measured frequency shift is seen to agree with that calculated from the thick iris formula.

Tests on a second cavity of approximately the same dimensions substantially confirmed the above result.

(i) The actual mean cavity dimensions as given in part IV (section 2) are probably correct to 1 part in

5000 or so. The ideal resonance frequency in vacuo is then, from (2.1), 8910.1 megacycles. To get the actual resonance frequency in air we must subtract:

2.80 Mc for the shift from vacuum to air

1.15 Mc for the shift due to the coupling holes

0.15 Mc for the shift due to finite conductivity.

The expected resonance frequency in air at room temperature is thus 8906.0 ± 2.0 megacycles. The actual resonance frequency (about 8907.1 megacycles) was well within that range.

2. Technique and Precautions

To obtain accurate and consistent results for the velocity of light a number of precautions had to be observed. The cavity was first carefully washed with a detergent, rinsed with water and dried. It was then assembled, connected into the frequency measuring apparatus, and allowed to reach room temperature.

The resonance frequency of the cavity was then measured, both in air and in vacuo, by comparison with the crystal standard as described in part IV and in the last section under (f). The crystal was compared to WWV at the same time. Readings were taken of temperature, pressure, and dew point. The frequency shift calculated from (6.2) was then compared to the measured value.

After the frequency measurement, the cavity was carefully sealed with a beeswax-rosin mixture. One of the coupling holes was closed with a brass plug and the glass capillary was connected to the other iris (Figs. 5 and 6). The cavity was clamped to a metal stand and the capillary tube and side arm were also held rigidly by clamp supports while the wax seal was completed. This was necessary to avoid breaking the seal when the stop cocks were turned and when the hose connection to the vacuum pump was attached to the side arm.

Some distilled water was boiled and poured into 125-milliliter flasks ready for weighing. The flasks were stoppered and kept closed throughout the test except for a short time when the cavity was filled. The amount of evaporation was not more than 1 milligram per hour.

The apparatus was then left over-night to reach temperature equilibrium, and a series of volume measurements were made the following day using the procedure outlined in part IV (section 3). The flasks containing distilled water were weighed just before and just after filling the cavity. A chemical precision balance was used for that purpose. The set of weights was checked for internal consistency and one of the weights was compared to a National Bureau of Standards weight.

Before each volume measurement room temperature, water temperature, barometric pressure and dew point were recorded. These data were used to compute the correction for buoyancy in air. This correction amounts to about 0.1% for water weighed against brass weights and can be calculated from

$$W_t = W_m\left[1 + \left(\frac{1}{\gamma_W} - \frac{1}{\gamma_B}\right)\gamma_A\right] \tag{6.3}$$

where

W_t is the "true" weight in vacuo

W_m is the measured weight in air

γ_W, γ_B, γ_A are the densities of water, brass, and air. The density of the brass weights was assumed to be 8.44 grams per cubic centimeter. The density of the air depends on atmospheric conditions but the dependency is not too critical (33). The buoyancy correction can be computed to 1 milligram if the barometric pressure is known to $\pm$ 10 mm Hg, the room temperature to $\pm 2°C$, and the dew point to $\pm 5°C$. However, the room temperature must be known to a fraction of a degree because of the large coefficient of expansion of water: about 1 part in 5000 per degree centigrade at room temperature (34).

The excess volume in the capillary tubing was then determined in a similar manner, except that some of the precautions were unnecessary because of the smallness of this volume.

When the velocity of light was computed from the average of a series of volume determinations and the corresponding frequency measurement, it was found that the results were consistently low by about the same amount. It was suspected that the cavity was not completely evacuated before it was filled with water. The residual air then occupied a small fraction of the cavity volume at approximately atmospheric pressure. This was verified by replacing the mercury manometer by a more sensitive

Pirani gauge and an oil manometer. By measuring the residual pressure a correction to the volume could be made which eliminated the discrepancy.

3. Results

The results of two series of measurements on the preliminary brass cavity are given in the following table:

	Series I	Series II
Corrected resonance frequency (reduced to vacuum)	8911.26 Mc at 24.4°C	8911.30 Mc at 25.0°C
Corrected volume measurements (reduced to temperature of corresp. frequ. measurement)	57.778 cm^3 57.770 cm^3 57.775 cm^3	57.773 cm^3 57.768 cm^3 57.766 cm^3
Mean of volume measurements	57.774 cm^3	57.769 cm^3
Value of c calculated from mean of volume measurements	299,767 km/sec	299,760 km/sec

A typical set of data and its reduction is shown below:

Frequency measurement

Barometric pressure: 746 mm Hg

Temperature: 24.4°C

Dew point: 13°C (corresp. saturation pressure P_w = 13.6 mm Hg)

Resonance frequency in air: 8907.08 Mc

Shift in frequency from air to vacuum (measured): 2.60 Mc

Volume measurement

Barometric pressure: 748 mm Hg

Temperature: 22.1°C

Dew point: 15°C

Residual pressure in cavity before filling: 0.9 mm Hg

Weight of flask before filling cavity: 159.102 g

Weight of flask after filling cavity: 101.314 g

Net weight of water: 57.788 g

Excess volume in capillary tubing: 0.248 cm^3

Excess volume in coupling irises: 0.033 cm^3

Reduction of frequency measurement

Resonance frequency in air (measured)	8907.08 Mc
Frequency shift to vacuum (calculated)*	2.88 Mc
Correction due to coupling irises	1.15 Mc
Correction due to finite conductivity of walls	0.15 Mc
Ideal resonance frequency in vacuo at 24.4°C	8911.26 Mc

Reduction of volume measurement

Measured weight of water at 22.1°C	57.788 g
Buoyancy correction	0.060 g
Correction due to residual pressure	0.071 g
Corrected weight	57.919 g
Total volume (γ_W=0.997747 g/cm^3 at 22.1°C)	58.049 cm^3
Correction for capillary tubing	-0.248 cm^3
Correction for coupling irises	-0.033 cm^3
Correction to 24.4°C	0.007 cm^3
Net cavity volume at 24.4°C	57.775 cm^3

* The calculated rather than the measured value was used (see VII)

VII. Discussion

1. Evaluation of accuracy

The following table lists the estimated limits of accuracy for the various measured and calculated quantities, and the corresponding uncertainty in the determination of the velocity of light.

	Limit of accuracy	Uncertainty in c
Resonance frequency in air	±0.05 Mc	2 km/sec
Measured shift from air to vacuum	0.30 Mc	12 km/sec
Calculated shift from air to vacuum	±0.10 Mc	4 km/sec
Correction due to coupling irises	±0.10 Mc	4 km/sec
Correction due to finite conductivity	±0.01 Mc	negligible
Ideal resonance frequency (using the calculated shift to vacuum)	±0.15 Mc	6 km/sec
Buoyancy correction	±0.6 mg	1 km/sec
Residual pressure	±0.1 mm Hg	12 km/sec
Density of water (assuming temp. is known to 0.2°C)	$\pm 46\times10^{-6}$ g/cm^3	4 km/sec
Excess volume in capillaries	±0.0005 cm^3	1 km/sec
Excess volume in irises	±0.0005 cm^3	1 km/sec
Temperature correction	±0.0005 cm^3	1 km/sec
Net cavity volume	±0.007 cm^3	13 km/sec
Uncertainty in final result		15 km/sec

The main uncertainty in the frequency measurement arises from the fact that the shift in resonance frequency from air to vacuum could not be measured too accurately because of the non-linearity in the frequency sweep (part VI, section 1f). The corresponding calculated value, on the other hand, is probably correct to within a few per cent because its dependence on atmospheric conditions is not too critical, as was pointed out previously. The calculated value therefore, was used in the reduction of of the frequency measurements.

Although the formulas for the frequency shift due to the coupling irises are probably quite rigorous, a deviation of ±10% was allowed for, to account for possible inaccuracies in the irises. An error of 0.005 inches in the hole diameters (about 3%) would give rise to such a deviation.

Considerable uncertainty in the volume measurement was introduced by the large residual pressure. Although this pressure could be read to within ±5%, the reliability of this measurement is rather doubtful. It is possible that part of the residual pressure is due to a small amount of water vapor. The limit of accuracy was therefore set at about ±10%.

The density of distilled water is quite accurately known, but to obtain a precision of 1 part in 50,000 for the cavity volume, the water temperature must be ascertained to $0.1^{\circ}C$. The room temperature could certainly be measured to that accuracy and stayed within 0.1°C during any one test. The water was at room temperature before the cavity was filled and after it was emptied, but the question arises whether or not its temperature changed slightly during the filling process due to initial evaporation into the evacuated cavity. It is believed that this effect is extremely small. Only a little water will evaporate initially. It must condense very rapidly immediately afterwards, so that the residual temperature change cannot be too large. This reasoning was confirmed by examining the tip of the capillary for emerging droplets after filling the cavity.

From the above discussion, it appears reasonable to set the accuracy of the preliminary result for the velocity of light at about $\pm$15 km/sec. Using the average result from part VI, we may write

$$c = 299{,}764 \pm 15 \text{ km/sec}$$

This is somewhat lower than Michelson's result, but is in substantial agreement with that result within the limits of experimental error.

2. Accuracy Attainable

The two main uncertainties in the frequency and volume determinations (see the tabulation in the last section) can undoubtedly be eliminated. The cavity should be machined to the specified dimensions to closer tolerances to bring its resonance frequency *in vacuo* directly within the range of the frequency standard. As an alternative, the latter could be redesigned to cover a wider frequency range. The vacuum system must be improved to obtain pressures as low as 10^{-2} or 10^{-3} mm Hg.

The cavity should be made more uniform in diameter and length. The variations in these dimensions should be kept within 1 or 2 tenthousandths of an inch to keep possible residual frequency shifts negligible (part V, section 3). Preferably, the cavity should be of steel and very carefully ground and polished. The coupling holes should be accurately reamed and counterbored.

The frequency measurements could be further improved by increasing the local oscillator power by a factor of ten or more. This would allow a reduction in the size of the coupling irises and in the frequency shift produced by them. The use of a more sensitive detector will also be a step in the same direction. There are, of course, limitations due to noise, microphonics, and stray pick-up, but there is still room for improvement with proper amplifier design and careful shielding.

The ultimate limit of accuracy of the method seems to be determined by the volume measurement. Refinements in apparatus and technique are possible. The entire experiment could be performed at or near 4°C to eliminate the uncertainty in the density of water.

From the above, it appears that an accuracy of 1 part in 150,000 may eventually be achieved by this method.

Appendix A

Principal Symbols Used

The rationalized M.K.S. system is used throughout.

Vectors are indicated by a bar underneath the letter, and complex numbers and their conjugate by the symbols ($\check{}$) and ($\hat{}$) above the letter.

$\underline{A}$ magnetic vector potential

$\underline{A}^o$ normalized vector potential

a subscript referring to the a th cavity mode

a wide dimension of wave guides

$\underline{a}_r, \underline{a}_\varphi, \underline{a}_z$ unit vectors in cylindrical coordinates

$\underline{B}$ magnetic induction

$\underline{B}^o$ normalized magnetic field

$\underline{B}_o$ magnetic exciting field at iris

$\underline{B}(0)$ magnetic field at center of iris

b narrow dimension of wave guides

C amplitude of wave guide fields

c velocity of light

c radius of coupling irises

D diameter of cavity

$\underline{E}$ electric field intensity

$\underline{E}^o$ normalized electric field

f resonance frequency of cavity

$\underline{H}$ magnetic field intensity

$\underline{i}, \underline{j}, \underline{k}$ unit vectors in rectangular coordinates

j square root of -1

k_{01} cut-off phase constant for TE_{01} mode in circular guide

L length of cavity

M magnetic polarizability of iris

$\underline{n}$ unit normal vector to cavity surface

p_a amplitude of a th cavity mode

Q_a' loaded cavity Q for the a th mode

Q_a unloaded cavity Q for the a th mode

R radius of cavity

R_s skin-effect surface resistance

r_{on} n th root of $J_0'(x) = 0$

S surface of cavity

S_1 area of input iris

S_2 area of output iris

V cavity volume

β wave number $2\pi f/c = \omega\sqrt{\mu\varepsilon}$

δ skin depth

ε dielectric constant of free space

ε_r relative dielectric constant of air

ξ, ζ, φ oblate spheroidal coordinates

η intrinsic impedance of air or free space $\sqrt{\frac{\mu}{\varepsilon}}$

λ wave length

μ permeability of free space

ρ length-to-diameter ratio of cavity

σ conductivity of material of cavity surface

ω angular frequency

Appendix B

Iris Calculations

To evaluate the coefficients A_n in (5.52), equation (5.56) was written for six points along the edge of the iris (A-B in Fig. 12). The radius c of the iris was taken equal to one to simplify the numerical work. The points were chosen at $\zeta = -0.1$, -0.2, -0.3, -0.4, -0.5, and -1.0. The corresponding values of ξ and of the cylindrical coordinates, ρ and z, were calculated from the relations

$$z = \zeta \xi \tag{B.1}$$

$$\rho = (1+\zeta^2)^{1/2}(1-\xi^2)^{1/2} \tag{B.2}$$

$$\rho = 1 - z = 1 + |z| \qquad (45^\circ \text{ cone}) \tag{B.3}$$

These equation can first be solved for z:

$$z = -\frac{\zeta^2}{2\zeta^2+1}\left\{\sqrt{2(1+\zeta^2)} - 1\right\} \tag{B.4}$$

ξ and ρ can then be found from (B.1) and (B.3).

Tables of integrals of associated Legendre functions were available (35). So were tables of $\frac{d}{d\zeta}P_n^1(j\zeta)$ and $\frac{d}{d\zeta}Q_n^1(j\zeta)$ for positive values of ζ (31). The corresponding values for negative ζ's were deduced from the series definitions of the general associated Legendre functions (36). They are

$$j^{-n} P_n^1(jx) = \frac{\sqrt{x^2+1}}{2^n} \sum_{r=0}^{[\frac{n-1}{2}]} \frac{(2n-2r)!\, x^{n-2r-1}}{r!(n-r)!(n-2r-1)!} \tag{B.5}$$

$$j^{n+1} Q_n^1(jx) = (-1)^n \left\{ j^{-n} P_n^1(jx)\left[\frac{\pi}{2} - \tan^{-1}x\right] + G(x) + H(x) \right\} \tag{B.6}$$

where

$$G(x) = \frac{-j^{-n} P_n(jx)}{\sqrt{1+x^2}} \tag{B.7}$$

$$H(x) = \sum_{r=0}^{[\frac{n-1}{2}]} \frac{(-1)^{n+1}(2n-1-4r)}{(2r+1)(n-r)}\, j^{-n+1+2r} P_{n-1-2r}(jx) \tag{B.8}$$

Substituting -x for x in the above relations, one obtains for odd values of n:

$$P_n^1(-jx) = P_n^1(jx) \tag{B.9}$$

$$Q_n^1(-jx) = -Q_n^1(jx) - j\pi P_n^1(jx) \tag{B.10}$$

By a similar substitution in the derivatives of (B.5) and (B.6):

$$\frac{d}{dx} P_n^1(-jx) = -\frac{d}{dx} P_n^1(jx) \tag{B.11}$$

$$\frac{d}{dx} Q_n^1(-jx) = -\frac{d}{dx} Q_n^1(jx) - j\pi \frac{d}{dx} P_n^1(jx) \tag{B.12}$$

All the terms in (5.56) can now be calculated numerically. The six points chosen yield the equations

$$.004128 + .08905\, A_1 + .6808\, A_3 + 2.0879\, A_5 + 4.7429\, A_7 = 0$$
$$.016111 + .18650\, A_1 + 1.8083\, A_3 + 6.7163\, A_5 + 18.2510\, A_7 = 0$$
$$.034965 + .28859\, A_1 + 3.4879\, A_3 + 15.475\, A_5 + 49.369\, A_7 = 0$$
$$.058724 + .38796\, A_1 + 5.7869\, A_3 + 30.236\, A_5 + 111.112\, A_7 = 0$$
$$.086209 + .48574\, A_1 + 8.8093\, A_3 + 53.367\, A_5 + 220.746\, A_7 = 0$$
$$.231253 + .89177\, A_1 + 34.854\, A_3 + 358.65\, A_5 + 1172.44\, A_7 = 0$$

The first four equations, when solved for the coefficients A_n, lead to the values given in the last section of part V. With these solutions, the first four equations are satisfied to four significant figures, the last two equations to three significant figures.

Appendix C

Evaluation of Polarizability of Iris

To find the magnetic polarizability for the thick iris, the integrals in equation (5.60) must be evaluated. The first term in the summation, $n=1$, has already been worked out for the thin iris. It can be easily shown that all other terms vanish and do not contribute to the polarizability of the iris.

For simplicity, we may again take $c=1$. In the plane of the iris ($\zeta=0$) we then have from (5.32)

$$\xi = \sqrt{1-\rho^2} = \sqrt{1-x^2-y^2}$$

Using the relations

$$\frac{d}{d\xi}P_1(\xi) = P_1'(\xi) = 1$$

$$P_3'(\xi) = \frac{3}{2}(5\xi^2-1)$$

$$P_5'(\xi) = \frac{15}{8}(21\xi^4-14\xi^2+1)$$

$$P_7'(\xi) = \frac{7}{16}(429\xi^6-495\xi^4+135\xi^2-5)$$

the integrals

$$\int_0^x \frac{d}{d\xi} P_n(\xi) \frac{x\,dx}{\xi}$$

can be evaluated (37). The resultant expressions are functions of ξ only, and hence the further integrations in (5.60) are straight-forward. When the latter are carried out, all terms vanish identically with the exception of the first one.

References

(1) Ladenburg, R., Handbuch der Experimentalphysik, 18 (1928) 1.

(2) Wolfsohn, G., Handbuch der Physik, 19 (1928) 895.

(3) Birge, R.T., Nature, 134 (1934) 771.

(4) Gheury de Bray, M.E.J., Nature, 120 (1927) 404, 594, 602.

(5) Michelson, A.A., Astrophysical Journal, 65 (1927) 1.

(6) Michelson, A.A., F.G. Pease, and F. Pearson, Astrophysical Journal, 82 (1935) 26.

(7) Mittelstaedt, O., Physikalische Zeitschrift, 30 (1929) 165.

(8) Anderson, W.C., Review of Scientific Instruments, 8 (1937) 239.

(9) Anderson, W.C., Journal of the Optical Society of America, 31 (1941) 187.

(10) Rosa, E.B., and N.E. Dorsey, Bulletin of the U.S. Bureau of Standards, 3 (1907) 433.

(11) Birge, R.T., Reviews of Modern Physics, 1 (1929) 1.

(12) Birge, R.T., Reviews of Modern Physics, 13 (1941) 233.

(13) Mercier, J., Journal de physique et le radium, 5 (1924) 168.

(14) Essen, L., Nature, 159 (1947) 611.

Essen, L., and A.C. Gordon-Smith, Proceedings of the Royal Society (London), 194 (1948) 348.

(15) Ramo, S., and J.R. Whinnery, Fields and Waves in Modern Radio, 1944, New York, Wiley, p. 402.

(16) Moreno, T., Microwave Transmission Design Data, 1948, New York, Mc Graw-Hill, p. 210.

(17) Gaffney, F.J., I.R.E. Proceedings, 34 (1946) 775.

(18) U.S. Department of Commerce, National Bureau of Standards Letter Circular LC-780, February 26, 1945.

(19) Sperry Gyroscope Company, Klystron Technical Manual, 1944.

(20) Slater, J.C., M.I.T. Radiation Lab Report 43-16, December 31, 1942.

(21) Condon, E.U., Journal of Applied Physics, 12 (1941) 129.

(22) Reference 15, p. 209.

(23) Bernier, J., L'Onde Électrique, 26 (1946) 3.

(24) Bethe, H.A., M.I.T. Radiation Lab Report 43-22, March 24, 1943.

(25) Bethe, H.A., M.I.T. Radiation Lab Report 43-30, April 9, 1943.

(26) Smythe, W.R., Physical Review, 72 (1947) 1066.

(27) Bethe, H.A., Physical Review, 66 (1944) 163, discussion 351.

(28) Smythe, W.R., Static and Dynamic Electricity, 1939, New York, Mc Graw-Hill, p. 157.

(29) Bethe, H.A., M.I.T. Radiation Lab Report 43-16, March 16, 1943.

(30) Smythe, W.R., Unpublished Notes

(31) Tables of Associated Legendre Functions, 1945, New York, Columbia University Press.

(32) Huston, B.F., and H. Lyons, A.I.E.E. Technical Paper 48-49, December 1947, p. 10.

(33) Hodgman, C.D., Handbook of Chemistry and Physics, 26th ed., 1942, Cleveland, Chemical Rubber Co., p. 1612.

(34) Reference 33, p. 1609.

(35) Prévost, G., Tables et Formules de Fonctions Sphériques et de leurs Intégrales, 1933, Paris, Gauthier-Villars.

(36) Reference 31, p. 137 and p. 181.

(37) Dwight, H.B., Tables of Integrals, 1947, New York, Macmillan, formulas 321.01 and 351.9.